THE IMPACT OF HYBRID ENERGY STORAGE ON POWER QUALITY, WHEN HIGH POWER PULSED DC LOADS ARE OPERATED ON A MICROGRID TESTBED

by

JAY PAUL KELLEY

Presented to the Faculty of the Graduate School of
The University of Texas at Arlington in Partial Fulfillment
of the Requirements
for the Degree of

MASTER OF SCIENCE IN ELECTRICAL ENGINEERING

THE UNIVERSITY OF TEXAS AT ARLINGTON

May 2014

Copyright © by Jay Paul Kelley 2014

All Rights Reserved

Acknowledgments

I would like to express gratitude to my advisor Dr. David Wetz for the support of my Master's studies and research. His motivation and enthusiasm produced an active lab work environment that was gratifying. His guidance forged better writing in all of his students, including myself. I believe I could not have had a better mentor or advisor for my graduate research at the university.

I would like to thank the students working in Dr. Wetz's lab for the memorable and enjoyable experience; Peter Novak, Biju Shrestha, James Reed, Caroline Storm, Travis Least, Isaac Cohen, Clint Gnegy-Davidson, Greg Turner, Anthony Matasso, Simon Donahue , and Matt Martin. In particular I would like to express my sincere gratitude towards my colleagues Isaac Cohen and Caroline Storm who also found themselves greatly involved in the MicroGrid, and James Reed for first introducing me to Dr. Wetz.

Finally, I would like to think my parents Donna and Danny Kelley for their love and guidance throughout my life as well as instilling the importance of education in me for college, graduate work and even more importantly continued lifelong learning.

December 03, 2013

Abstract

THE IMPACT OF HYBRID ENERGY STORAGE ON POWER QUALITY,
WHEN HIGH POWER PULSED DC LOADS ARE OPERATED
ON A MICROGRID TESTBED

Jay Paul Kelley, M.S.

The University of Texas at Arlington, 2014

Supervising Professor: David A. Wetz

As the Navy's demands for high power transient loads evolves, so too does the need for alternative energy sources to back-up the more traditional power generation. Such applications in need of support include electrical grid backup and directed energy weapon systems such as electromagnetic launchers, laser systems, and high power microwave generators, among others. Among the alternative generation sources receiving considerable attention are energy storage devices such as rechargeable electrochemical batteries and capacitors. In such applications as those mentioned above, these energy storage devices offer the ability to serve a dual role as both a power source to the various loads as well high power loads themselves to the continual generation when the high power transient loads are in periods of downtime. With the recent developments in electrochemical energy storage, lithium-ion batteries (LIBs) seem like the obvious choice, but previous research has shown that the elevated rates of charging can be detrimental to both the cycle life and the operational life span of the device. In order to preserve the batteries, their charge rate must be limited. One proposed method to accomplish the dual role task mentioned above, while preserving the life of

the batteries, is by combining high energy density LIBs with high power density electric double layer capacitors (EDLCs) or lithium-ion capacitors (LICs) using controllable power electronics to adjust the flow of power to and from each device. Such a configuration is typically referred to as hybrid energy storage module (HESM). While shipboard generators start up, the combined high energy density and high power density of the HESM provides the capability to source critical loads for an extended period of time at the high rates they demand. Once the generator is operationally efficient, the HESM can act as a high energy reservoir to harvest the energy from the generator while the loads are in short periods of inactivity. This enables the generator to maintain its operation at levels of high efficiency thereby increasing the power quality of the AC bus. The work discussed here is aimed at evaluating how the use of energy storage impacts the power quality on MicroGrid's AC bus when high rate DC and AC loads are sourced simultaneously. Also HESM has been developed and evaluated as a mean to optimizing both the power and energy density of the energy storage installed.

Table of Contents

Acknowledgements iii

Abstract iv

List of Illustrations viii

List of Tables xi

Chapter 1 Introduction 1

Chapter 2 Background 3

2.1 Applications 3

2.2 Power Electronics 11

2.3 Energy Storage 15

2.3.1 *Flywheels* 16

2.3.2 *Fuel Cells* 18

2.3.3 *Batteries* 20

2.3.4 *Capacitors* 23

Chapter 3 Experimental Setup 30

3.1 Power Quality Impact Experimental Setup 42

3.2 Experimental Setup for Evaluating a COTS HESM on Power Quality 47

Chapter 4 Experimental Results 55

4.1 Power Quality when Sourcing Pulsed Loads without a HESM 55

4.2 Evaluation of the COTS HESM with Pulsed Loads on Power Quality 71

Chapter 5 Summary and Conclussions 82

References 84

Biographical Information 88

List of Illustrations

Figure 2.1 Ship Power Architectures 5
Figure 2.2 Zonal Ship Architecture 8
Figure 2.3 Power Quality Transient Response Standards for Naval Vessels 10
Figure 2.4 Ideal Buck and Boost Converters 12
Figure 2.5 Passive and Cascaded HESM 14
Figure 2.6 Full Active HESMs 14
Figure 2.7 Ragone Plot of Energy Storage Technologies 16
Figure 2.8 Flywheel Cross-Sectional Diagram 18
Figure 2.9 SOFC Reaction Cross-Section 19
Figure 2.10 Battery Reactions 22
Figure 2.11 EDLC Operation 25
Figure 2.12 Visual comparisons of EDLC and LIC 27
Figure 2.13 Time Averaged Current 28
Figure 3.1 UTA MicroGrid 31
Figure 3.2 UTA MicroGrid Relay & Switch Schematic 36
Figure 3.3 UTA MicroGrid Renewable Installation 36
Figure 3.4 UTA MicroGrid Image 37
Figure 3.5 UTA MicroGrid 1 Bus Image 37
Figure 3.6 UTA MicroGrid Power Electronics 38
Figure 3.7 UTA MicroGrid Fuel Cell 38
Figure 3.8 National Instruments CompactRio 40
Figure 3.9 UTA MicroGrid 1 Power Quality Setup 43

Figure 3.10 COTS HESM Circuit Diagram 48
Figure 3.11 COTS HESM Physical Setup 48
Figure 4.1 Energy Storage V&I for 300 W Load Experiment 56
Figure 4.2 Energy Storage V&I for 1300 W Load Experiment 57
Figure 4.3 Energy Storage V&I for 2000 W Load Experiment 58
Figure 4.4 Charger Output Current during the 300 W Experiment. 58
Figure 4.5 Charger Output Current during the 1300 W Experiment. 59
Figure 4.6 Charger Output Current during the 2000 W Experiment. 59
Figure 4.7 Programmable Load Voltage during 300 W Load Experiment 60
Figure 4.8 Programmable Load Voltage during 1300 W Load Experiment 61
Figure 4.9 Programmable Load Voltage during 2000 W Load Experiment 61
Figure 4.10 Generator Voltage during the 300 W Load Experiment 62
Figure 4.11 Generator Voltage during the 1300 W Load Experiment 62
Figure 4.12 Generator Voltage during the 2000 W Load Experiment 63
Figure 4.13 Programmable Load Current during the 300 W Load Experiment 63
Figure 4.14 Programmable Load Current during the 1300 W Load Experiment 64
Figure 4.15 Programmable Load Current during the 2000 W Load Experiment 64
Figure 4.16 Generator Current during the 300 W Load Experiment 65
Figure 4.17 Generator Current during the 1300 W Load Experiment 65
Figure 4.18 Generator Current during the 2000 W Load Experiment 66
Figure 4.19 HESM Bus Voltages 72
Figure 4.20 HESM System Currents 73
Figure 4.21 HESM Energy Storage Unregulated Currents 74
Figure 4.22 HESM Unregulated Bus Voltages 75
Figure 4.23 HESM System Currents for Unregulated Recharge 76
Figure 4.24 HESM Discharge Currents 77

Figure 4.25 HESM Discharge Voltages 79
Figure 4.26 HESM Recharge Voltages 79
Figure 4.27 HESM System Currents with Recharge Regulation 80
Figure 4.28 HESM Single Pulse Power Flow 81

\

List of Tables

Table 2.1 Power Quality Standards for Shipboard IPS 9

Table 3.1 Distributed Energy Sources Specifications 35

Table 3.2 Charge Controller and Inverter Specifications 35

Table 3.3 UTA MicroGrid NI CompactRIO Specifications 42

Table 4.1 Generator and AC Load RMS Voltages for 2 s 100% Duty Load Profile 67

Table 4.2 Generator Power Quality Analysis for 2 s 100% Duty Load Profile 67

Table 4.3 Programmable AC Load Power Quality Analysis for 2 s 100% Duty Load Profile 68

Table 4.4 Generator Power Quality Analysis for 30 ms 50% Duty Load Profile 68

Table 4.5 Programmable AC Load Power Quality Analysis for 30 ms 50% Duty Load Profile 69

Table 4.6 Generator Power Quality Analysis for 400 ms 50% Duty Load Profile 69

Table 4.7 Programmable AC Load Power Quality Analysis for 400 ms 50% Duty Load Profile ... 69

Chapter 1

Introduction

As the Navy's demands for high power transient loads evolves, so too does the need for alternative energy sources to back-up the more traditional power generation. Such applications in need of support include electrical grid backup and directed energy weapon systems such as electromagnetic launchers, laser systems, and high power microwave generators, among others. Among the alternative generation sources receiving considerable attention are energy storage devices such as rechargeable electrochemical batteries and capacitors. In such applications as those mentioned above, these energy storage devices offer the ability to serve a dual role as both a power source to the various loads as well high power loads themselves to the continual generation when the high power transient loads are in periods of downtime. With the recent developments in electrochemical energy storage, lithium-ion batteries (LIBs) seem like the obvious choice, but previous research has shown that the elevated rates of charging can be detrimental to both the cycle life and the operational life span of the device. In order to preserve the batteries, their charge rate must be limited. One proposed method to accomplish the dual role task mentioned above, while preserving the life of the batteries, is by combining high energy density LIBs with high power density electric double layer capacitors (EDLCs) or lithium-ion capacitors (LICs) using controllable power electronics to adjust the flow of power to and from each device. Such a configuration is typically referred to as hybrid energy storage module (HESM). While shipboard generators start up, the combined high energy density and high power density of the HESM provides the capability to source critical loads for an extended period of time at the high rates they demand. Once the generator is operationally efficient, the HESM can act as a high energy reservoir to harvest the energy from the generator while the loads are in short periods of inactivity. This enables the generator to maintain its operation at levels of high efficiency thereby increasing the power quality of the AC bus. The work discussed here is aimed at evaluating how the use of energy storage impacts the

power quality on MicroGrid's AC bus when high rate DC and AC loads are sourced simultaneously. Also HESM has been developed and evaluated as a mean to optimizing both the power and energy.

Chapter 2

Background

Typically, an energy storage device is either power dense or energy dense but not both. A HESM allows for the deployment of an energy storage system that maximizes both properties. Energy density is the amount of work that the device can perform when connected to a system divided by either the weight or volume of the device. Power density is the rate at which the energy can be transferred out of the device divided by the device's weight or volume. As mentioned before, the HESM concept is not a new one. Researchers have previously demonstrated small proof of concept experiments along with simple analytical models. Their results are reflected in the development of internal controls and configuration of the HESMs and the selection of energy storage devices. To better understand the significances of different design parameters and the system integration effects of a COTS HESM system, studies regarding the end use applications will be presented. Subsequently, developments in HESM research leading into the research presented here will be covered.

2.1 Applications

The development of hybrid energy storage technologies and topologies is guided by the primary end-use applications. One of the primary applications for which they have been considered thus far is that of the electric vehicle. Electric vehicles can range from personal cars and commercial trucks to oceanic naval and cargo ships. In recent years there has been a movement to develop and implement All-Electric Ships (AES). Thongam et al. [1] discuss reasons behind the drive toward the implementation of the AES and the sub-system aspects and options. The AES provides improved power generation efficiency for the ship. Traditionally, the propulsion system has utilized dedicated generators with direct mechanical connection to the propulsion through gear reduction. The loss of efficiency in this approach occurs in two areas. The first area of efficiency loss derives from the idea that the dedicated propulsion generators must be sized for the maximum cruising velocity. The result is that to operate

throughout a range of different cruising velocities the generators are not always able to be operated at maximum efficiency. The second area of efficiency loss is a result of having separated dedicated generators for propulsion and the shipboard electrical system.

An example of the traditional power and propulsion system of naval vessels can be found in the DDG-51 Arleigh Burke Class destroyers [2]. The Arleigh Burke Class has independent propulsion and electrical service systems. The propulsion system is powered by two LM2500 gas turbines that are mechanically connected to the propellers. The electrical system has two turbine-generators to provide electrical power, with a third for emergency backup. The total resulting power generation is 7.5 MW [2]. While the pure mechanical connection between the propeller and gas turbines is very efficient, the operational states of the turbines are limited. Finer control of speed is handled by adjustable pitch propellers. The propulsion system is designed to run optimally in a tactical situation, however most of the ship's lifespan will be spent at a much lower cruise speed. The reduced fuel efficiency of the propulsion system when operating at the lower cruise speed results in significant costs of operation [2]. An AES, such as the DDG-1000 Zumwalt Class destroyer, solves this problem by employing an Integrated Power System (IPS). The power generation of the Zumwalt class includes two Rolls-Royce MT30 main turbine generators and two Rolls-Royce 4500 auxiliary turbine generators for a total of 78 MW of power generation [3, 4]. By increasing the number of generators connected to the electrical power system and by the decoupling power to propulsion from generator operation, there exist more levels of power generation in which all active generators are operating at maximum efficiency. An illustration of the difference between the older power and newer IPS distribution connections are shown in Figure 2.1. While the number of efficient levels of power generation has been increased, there are still levels of loading on the IPS for which one or more generators would have to be moved out of optimal operation. Implementing HESMs in the Power Conversion and Distribution creates a partial decoupling of power generation and IPS load levels by acting as an efficient power source when the IPS

loading is above the local efficient operational state or as a load being recharged when the IPS loading is less than the nearby efficient power generation state. A prime advantage of the decoupling of power generation and shipboard loads is that the propeller speed can now be varied by simply adjusting the amount of power applied to the motors. As a result variable pitch blades are no longer needed. The primary tactical advantage is that fixed propeller designs are capable of more silent operation with respect to being detected by sonar [3]. The inclusion of HESMs in an IPS reduces the amount of needed mechanical redundancy in power generation. Rather than being forced to rely on quick start auxiliary power generators for momentary or catastrophic failure in the operation of the primary power generators, HESMs can be used to provide ship power until the momentary failure has passed or another primary power generator can be brought online. In a tactical situation, this supports the AES's ability to effectively withdraw from an engagement or swiftly complete operation objectives.

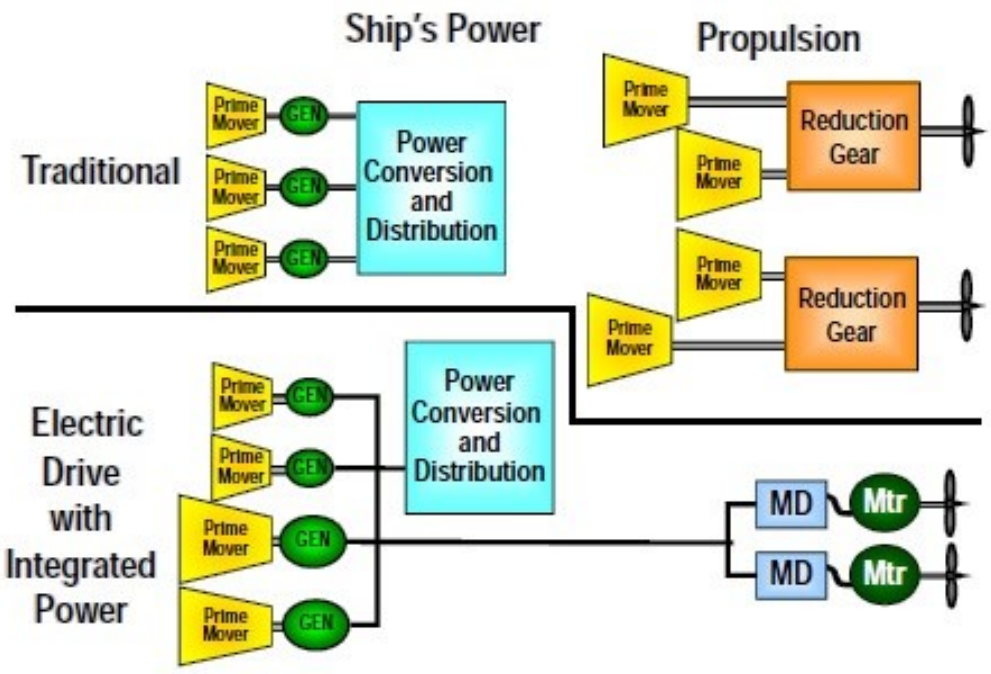

Figure 2.1 Ship Power Architectures illustration of power and propulsion comparing the older standard to the modern IPS [5].

Within the shipboard architecture, the IPS consists of a ship-wide electrical power transmission grid with various loads and generators connected to it throughout the ship's infrastructure. With regards to ship propulsion, the output, such as the propeller, can be moved by a motor system that is connected to the IPS. Not only do the generators no longer have to be located and aligned with the propulsion output, but different generators can be operated together to provide the current amount of needed power. This enables an increase in the number of total power generation operation levels at which individual generators are operating at maximum efficiency and as a result optimizes the unit commitment for a desired fuel economic dispatch. With a well implemented IPS the same principles of generator and load separation can also be applied to high power systems and their supporting HESMs as presented by Beach and McNab [6]. This allows for the weight of even heavy generators and HESMs to be manipulated for the benefit of the ship. While weight is normally a detracting factor in a system, it is not as prevalent of a concern if it can be integrated low in the ship along the center-line. In fact a ship's stability is increased and the weight of heavier weapon systems on the ship's deck can be offset. The safety of operation can be improved my placing potentially volatile energy storage if damaged in a section of the ship that is better protected against tactical and environmental threats than a location close to the load.

Even with an IPS, not all loads and energy storage devices can be readily separated, particularly high power pulsed loads. In such systems timing can vary from picoseconds to seconds and may require pulse shaping, which place limitations on the transmission distance between the energy storage and load. For example, the devices directly feeding the load may be a set of inductors and capacitors that both perform pulse shaping and provide the load with the energy at the needed rate for a single usage of the pulsed load. In this case, these devices must remain nearby the load. These devices are recharged via the prime power source, which is connected through power conversion electronics for a DC voltage transition. Depending upon the required recharge timeframe and line losses, which are dependent on the recharge rate, the

energy dense devices of the HESM may or may not be able to be located at a further distance from their power dense counterparts. High power and pulsed loads are becoming of increasing prevalence in both interest and usage aboard naval ships. These loads include, but are not limited to, electromagnetic launch assist of aircraft or projectiles, high power lasers, radars, and microwave generators. Some of the high power loads also require a baseline amount of power supplied. For example, the high power radar systems require a baseline power supply for passive detection and a high power pulsed supply for active tracking.

When designing the IPS to work under extreme conditions, the ability to supply load power while bypassing inoperable sections of the IPS is required. The result is that the next generation IPS takes on the form of many interconnected small zone electrical sub-systems. In each zonal section, a HESM can be used to provide either backup power for a generator in a zone or as the primary power source should the zone become isolated from a generator. A comparative figure of the traditional feeder based network approach and the zone based approach is shown in the following, Figure 2.2. Additionally, these concepts can also be applied to the electrical utility grid or MicroGrid interconnections which employ a feeder based approach, where redundancy is provided by the addition of many interconnecting transmission lines between the same nodes. The zonal approach for a utility grid relies less on the reliability of an individual node by interconnecting more nodes to provide alternative transmission pathways in the event of a fault [7].

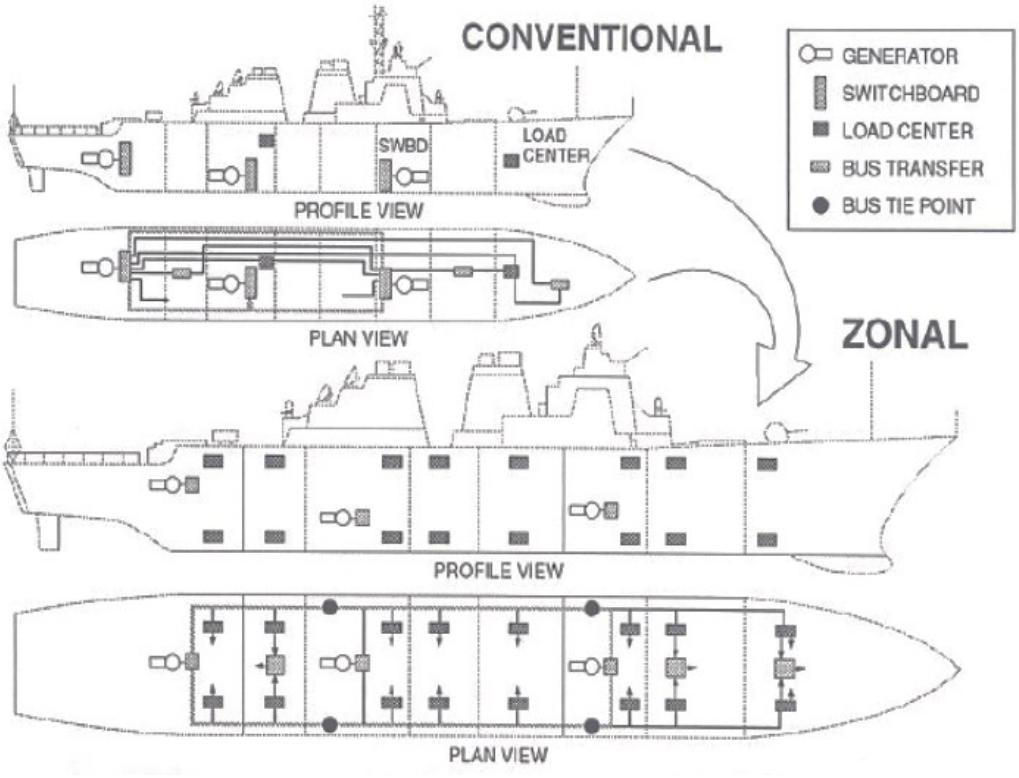

Figure 2.2 Zonal Ship Architecture: Main Electrical Bus layouts of feeder based (top) and zonal (bottom) distributions [7]

Through a combination of the various loads, power generation, and energy storage technologies, an AES is a floating and mobile MicroGrid. The zonal configuration of the AES is a set of interconnected MicroGrids. As in large land based electrical utility grids and MicroGrids, power quality is of great importance in an AES, as presented by Thongam [1]. The American Bureau of Shipping in conjunction with the Naval Sea Systems Command jointly developed standards for naval vessel power systems and utilized commercial standards when possible in order to simplify the standards. Among these standards are requirements for electrical system redundancy and power quality. The power quality standards for commercial vessels and naval vessels include a limit on the Total Harmonic Distortion, THD, of 5% and a limit on the relative magnitude of the power, magnitude, of any single harmonic with respect to the fundamental frequency of 3%. The THD is the sum of powers of all multiples of the fundamental frequency,

starting with the 2nd harmonic, divided by the power of the first harmonic, fundamental frequency, as given by: THD=$\frac{\sum_{i=2}^{\infty} P_i}{P_1}$. Additional aspects of power quality and their standards are shown below in Table 1 [7,8]. And the subsequent Figure 2.3, from one of the naval military standards regarding shipboard electrical systems, illustrates the meaning of the frequency and voltage transient response values and times.

Table 2.1 Power Quality Standards for Shipboard IPS [7,8]

Power Quality	Frequency Deviation	Frequency Transient	Voltage Deviation	Voltage Transient
Commercial	±5%	±10% for 5 secs	+6% to -10%	±20% for 1.5 secs
Naval	±3%	±4% for 2 secs	±5%	±16% for 2 secs

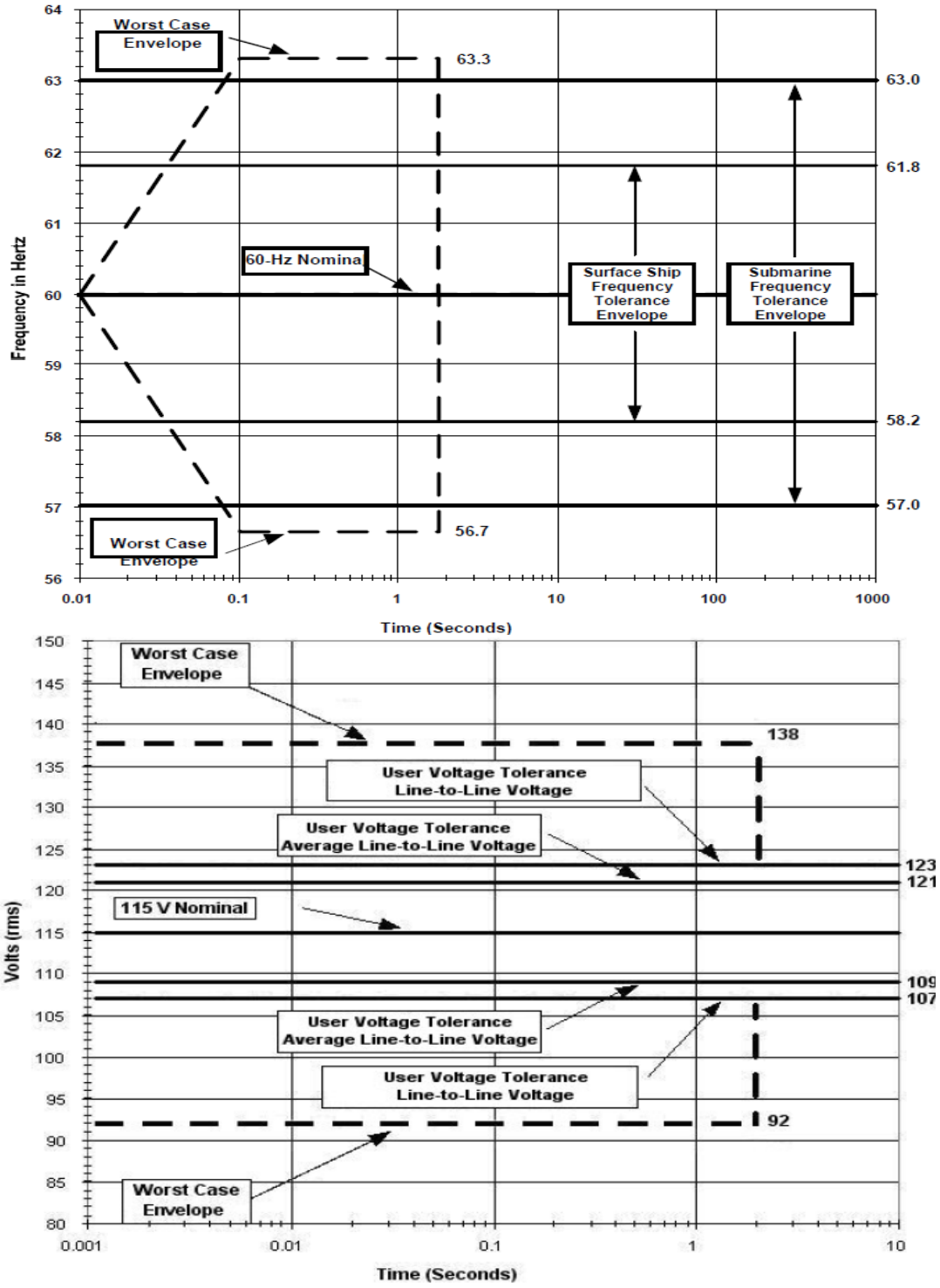

Figure 2.3 Power Quality Transient Response Standards for Naval Vessels [8].

Land based MicroGrid research and construction often includes the use of renewable energy sources. These sources produce power with a range of frequencies and magnitudes. Wind turbines are rotating machines that produce AC power, and are typically configured for three phase power. Fuel Cells and Photovoltaic cells produce various levels of unregulated DC power. In order for these sources to be connected to a common bus, the use of power electronic converters is required. The power quality in a MicroGrid is dictated by both the capabilities of the power source and that of all the power electronics between the source and the system bus of interest. If the primary power generation sources are providing insufficient power or power quality for a desired load then energy storage can be utilized to provide limited term support. The concept of letting energy storage handle spikes in loading and maintaining power generation at a constant rate is known as peak shaving. Adjusting the flow of current for the recharge of the energy storage in response to various peak load demands so that the load is supplied with power and the intermediate energy storage is not fully drained is dependent upon the time-averaged current of the energy storage.

2.2 Power Electronics

In a HESM where the different energy storage devices operate at different voltages, each one must have voltage regulator between it and the Point of Common Coupling (POCC) within the HESM. Similarly, voltage regulators may be needed between the HESM output or the load and the electrical utility or MicroGrid POCC. Since the energy storage module devices operate with Direct Current (DC) a simple transformer cannot be used for voltage regulation and adjustment, instead power electronic boost and buck converters are employed. Power electronics can also be used to control and limit the current flow from the sources during both discharge as well as recharge. The use of power electronics is not limited to within the HESM. In a MicroGrid platform where renewable sources are employed, additional power electronics are needed to match their unregulated output to the POCC. Power electronic converters have an initial delay in operation during which the internal capacitors and inductors are charged up

from zero state initial conditions to the desired partial energized state that corresponds to the input/output ratio.

Both the increase and decrease of voltage through the converters is achieved by utilizing the energy storage nature of inductors. Inductors store energy in a magnetic field and resist changes in current much like capacitors that store energy in an electric field and resist changes in voltage potential. The voltage induced across an inductor, V_L, is equal to the inductance times the derivative of current with respect to time, $V_L = L\frac{di}{dt}$. Converters use this developed inductor voltage potential to add in series with the input voltage of the source in the case of a boost converter. In the case of a buck converter, the induced inductor voltage is subtracted from the input source voltage. To employ this, the inductor circuit must be continuously operated in a transient state by operating the converter with a high switching frequency. Capacitors are used to stabilize the output voltage throughout switching cycles. A visual illustration of the switch states, current flows and voltage polarity of the inductors is given below in Figure 2.4.

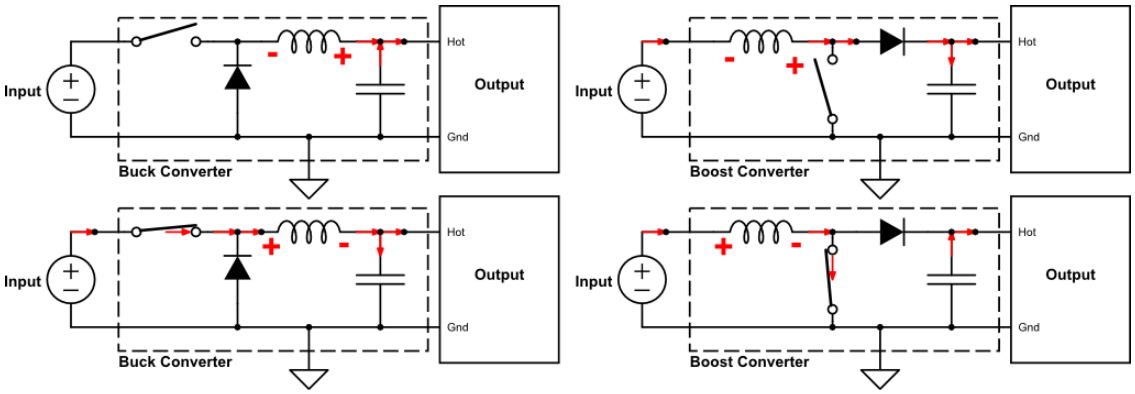

Figure 2.4 Ideal Buck Converter (left) and Ideal Boost Converter (right).

The top left buck converter image shows the energized capacitor providing current to the load while the capacitor applies the load voltage. The bottom left buck converter image shows the inductor and capacitor being recharged with the output current supplied by the input

and the output voltage being the difference between the input voltage and the present inductor voltage drop. To maintain a stable output voltage, the converter switching must be fast. The bottom left boost converter image shows the inductor being energized by the input to a high amp short circuit current, and the capacitor providing both the output voltage and current. The top right boost converter image shows a charged inductor boosting the input voltage and supplying both the load and capacitor with voltage and current.

Power electronics are used in the conversion from AC power to DC power as well as the reverse process. From this, it is easy to think that the management of a HESM or MicroGrid revolves solely around the internal control of the power electronics; however, this is not the case. The output voltages of most power electronic buck or boost converter topologies are based off of the input voltage multiplied by a gain. These converters also have a very specific input voltage ranges required for correct operation. Thusly, it is important to manage the energy storage devices as well, with emphasis on the voltage level seen by the power electronics. Unless the power electronic converter is capable of sinking a variable range of currents like an adjustable load, the current control of the converter with respect to the input or output current has a regulated upper limit as opposed to specific current output control. Utilizing power electronics to control voltages and currents in a HESM is referred to as active control. Khaligh and Li [9] show a variety of different topologies for an active HESM in reference to a passive HESM that lacks power electronics between energy storage devices, as shown in Figures 2.5 and 2.6. In these figures the two-quadrant DC/DC converter connected to the DC bus is representative of the step-up voltage conversion necessary to drive loads that operate at higher voltages than the energy storage. As mentioned previously this conversion can use either AC or pure DC conversion. In pure DC conversion, a step up DC/DC, boost converter is implemented. The AC version employs a DC to AC inverter which feeds a step up transformer followed by conversion back to DC. Depending on the available parts and components, the two-quadrant converters can be realized by separate boost and buck converters setup in anti-parallel. The

choice of power conversion methods is dependent upon the capabilities of commercially available products. “During the 1990s, the U.S. Government initiated a streamlining of government regulations which led to the evaluation of all military standards and specifications (MIL-STDs and MIL- SPECs). Additionally, the Department of Defense’s (DOD) Procurement Reform policies began to encourage maximum use of commercial standards and commercial-off-the-shelf (COTS) equipment” [7].

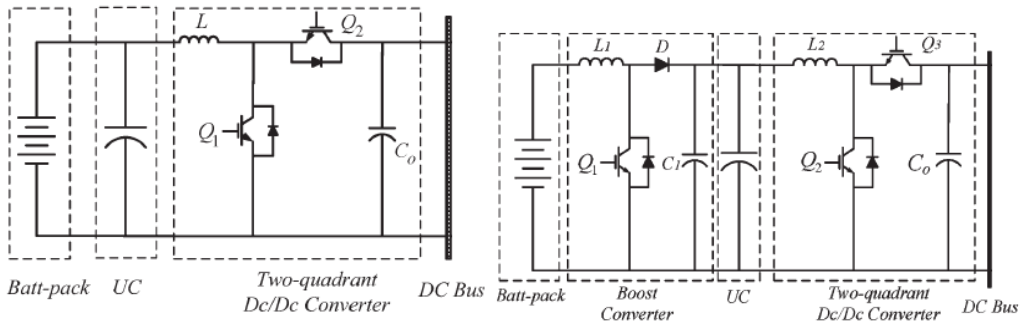

Figure 2.5 Passive and Cascaded HESM: Passive (left) with a direct connection between the battery and capacitor banks. Actively controlled battery bank cascaded to the capacitor bank (right) [9].

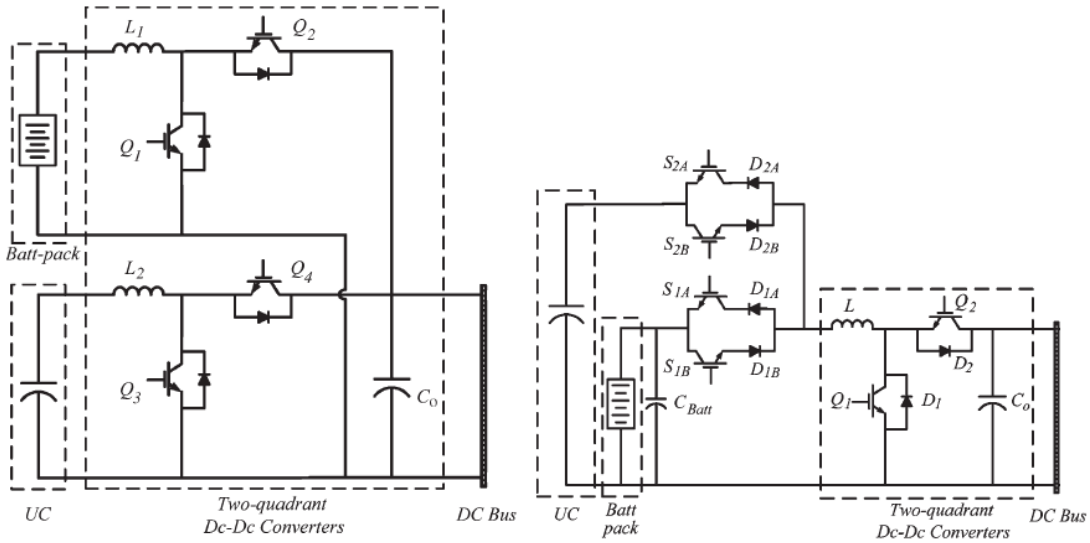

Figure 2.6 Full Active HESMs: Active control on both battery and capacitor banks (left). Actively controlled current direction flow with battery and capacitor banks coupled to common voltage node (right) [9].

While power electronic converters are not 100% efficient they are typically close, in the range of 90-98%. As a result there is a small drop in system power conversion efficiency. However, employing power electronics allows for the decoupling of voltage levels between energy storage technologies. This decoupling allows the power dense energy storage technologies to operate with greater independent efficiency. Capacitors are a prime example, the energy of a capacitor is $E = \frac{1}{2}CV^2$ and the usable energy, ΔE, comes from changes in voltage: $\Delta E = \frac{C}{2}(V_{initial}^2 - V_{final}^2)$ for discharge. Without power electronics the change in voltage of a capacitor would be limited to small transient changes about the voltage of the energy dense technology voltage.

Brandhorst and Chen [10] experimentally demonstrated that a battery and supercapacitor HESM is able to provide a more stable DC bus voltage and improve the power quality over the use of batteries alone. Gao et al. [11] demonstrated through both simulation and experimental verification at low voltage; that the capacitor can be successfully used to cover the pulsed load and that the battery, possibly in conjunction with a power supply, can be used to recharge the capacitor between pulsed load occurrences. Utilizing a base current limit from the battery that is the average of the constant base load and pulsed load, the capacitor can be successfully recharged if enough time is given between pulses.

2.3 Energy Storage

There exists a wide range of devices and means by which the energy storage can be implemented. The ones selected to be presented are those that have shown promise and been prevalent in research with regards to high power pulsed loads. These energy storage devices include flywheels, fuel cells, batteries, and intermediate storage such as capacitors and inductors. These various energy storage technologies have different energy and power densities, as can be seen in Figure 2.7. These densities coupled with different operational

behaviors and costs of deployment and operation are to be considered in the planning of the HESM.

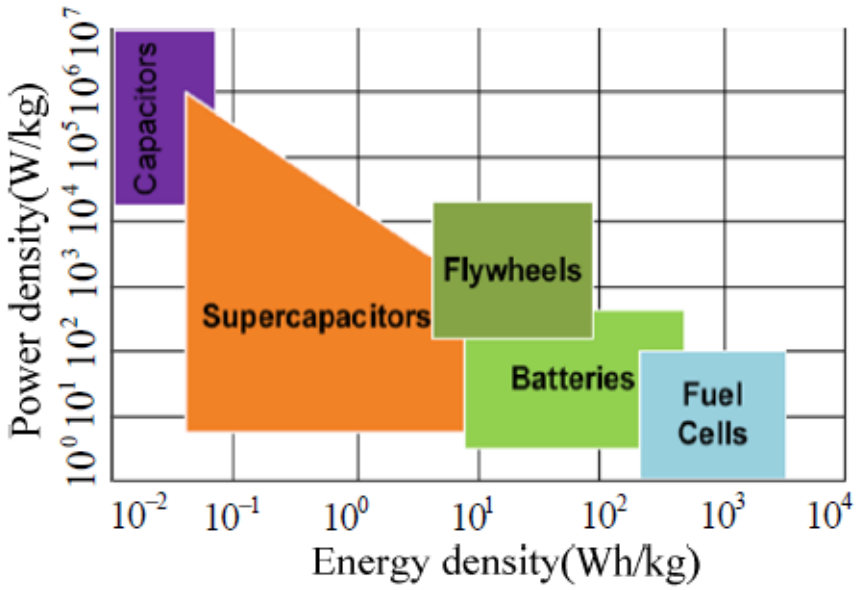

Figure 2.7 Ragone Plot of Energy Storage Technologies of common use [12]

2.3.1. Flywheels

Flywheels are the prevailing mechanical energy storage technology and store energy as rotational momentum. The maximum kinetic energy that can be stored in a flywheel is dependent upon the moment of inertia of the particular flywheel and the maximum achievable angular velocity. Rotational momentum is the product of the angular velocity and moment of inertia of a particular flywheel. The physical geometry and internal distribution of mass determine the moment of inertia. Energy is stored in the flywheel by using a motor to convert the electrical energy into a mechanical rotation. The motor increases the angular velocity of rotation. When a load is applied to the flywheel system via a connection to the motor, the motor changes its behavior and acts like a generator by transferring a portion of the rotational momentum of the flywheel back into electrical energy and leaving the flywheel with a decreased rotational momentum. The energy and power density of a flywheel are superb but are limited by the supporting equipment for the flywheel. This equipment includes the acceleration and

deceleration motor/generator(s), which are typically setup for high revolution per minute capability over torque to enable high rotational velocity connections. The energy density of a particular flywheel is limited only by maximum achievable angular velocity. The power density is affected by how much torque at the current rotation speed the connections can handle. With electrical based energy transfers, if the rate of change of energy is too much for the connection, slipping will occur and energy will no longer be extracted from the flywheel until the system synchronizes again. While flywheel systems do not require regular replacement like that of electro-chemical batteries, regular maintenance must still be performed. Vacuum seals, ball bearings, and the lubrication must be regularly checked and possibly replaced in order to ensure safe and efficient operation of the flywheel system. Other downsides to employing flywheel energy storage are the costs of fabricating and installing sufficient support structuring for the flywheel and power conversion machinery as well as the associated weight. Of particular interest are the support structure requirements with respect to usage in a HESM within an AES. An AES is subject to changes in pitch and roll in the open seas and in combat operations further system impact or vibrational shocks might be experienced by the vessel. The supporting structure for the flywheel is best served by being indirectly attached to the physical structure of the AES, so that the flywheel is not forced to change its angular velocity for all changes in the physical orientation of the ship which would result in a loss of energy in the flywheel. This loss of energy would be applied to the physical support beam of the flywheel and would result in the degradation of the beam, posing a potential risk hazard. The potential risks associated with ship movement and received shocks can be minimized by employing an isolated supporting structure for the flywheel capable of self-balancing and alignment to the flywheel rotational axis as well as by setting up the flywheel's axis of spin in parallel with the keel line of the AES [13].

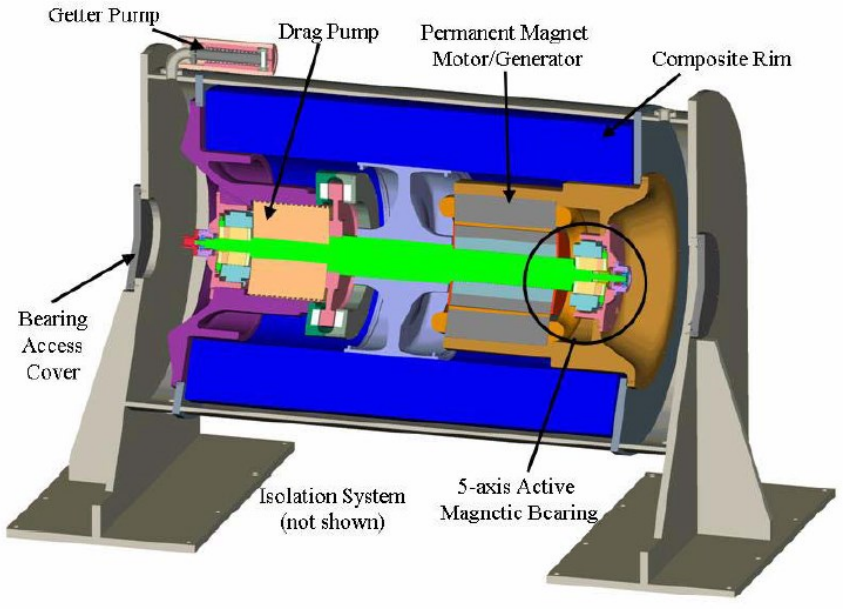

Figure 2.8 Flywheel Cross-sectional Diagram of a horizontally configured orientated [13]

2.3.2. Fuel Cells

Fuel Cells are another energy storage technology that can be employed in a HESM. A fuel cell operates as an energy source like a generator in that it takes fuel, hydrogen, and converts it to electricity. Fuel cells are devices that produce a continuous electric current directly from the oxidation of a fuel [14]. Different fuel cell electrolyte types have different operational characteristics. The name of a type of fuel cell comes from the type of material used as the electrolyte. For example, the proton exchange membrane fuel cell has fast start up and shut down times but low maximum operating power whereas the solid oxide fuel cell has significantly longer start up and shut down times but can be setup to provide power on the level of MW as would be needed in an AES [15]. Solid oxide fuel cells, SOFCs are among the fuel cell types that could be used in a HESM aboard an AES. In order to explain the operation of a fuel cell, the SOFC type will be used for example. The electrolyte is a solid oxide ceramic, often Yttria-stabilized zirconia (YSZ). The solid, dense, structure of the electrolyte prevents anodic or cathodic material to permeate through to the other side. On either side of the electrolyte exists an electrode. In order to increase the surface area for chemical reactions, the electrodes are

porous. In SOFCs the chemical reaction begins on the cathode side with the fuel on the cathode side being oxygen, O_2. The reaction is reduction with oxygen being consumed to form oxygen ions: $O_2 + 4e^- \rightarrow 2O^{2-}$ [16]. The electrolyte must be dense enough to keep the oxygen gas on the cathode side of the fuel cell as well as the hydrogen containing anode fuel on the anode side. The electrolyte must also have high conductivity for negative ions. After passing through the electrolyte, the negative oxygen ions react in the anode electrolyte with the anode fuel, hydrogen, to produce water and electrons: $2H_2 + O_2^{2-} \rightarrow 2H_2O + 4e^-$ [16]. The reaction is shown in Figure 2.9.

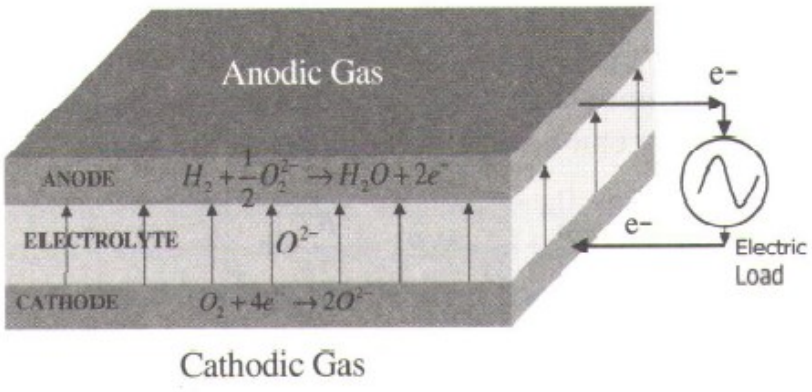

Figure 2.9 SOFC Reaction Cross-Section [16]

The energy density of the fuel cell is dependent on energy content of the fuel and its flow rate. The power density is dependent upon the surface areas of the internal membranes [17]. This allows the fuel cell to be selected as a reliable energy dense technology. The major drawback, as mentioned earlier, is the start-up time. Most of the electrolytes of SOFCs require high operating temperatures to maintain ionic conductivity. The turn on and turn off times are a result of this high temperature requirement, as it takes time for the fuel cell to raise the internal temperature of the electrolyte from ambient to the operational level or the reverse for shut down. The greater the temperature difference between ambient and operation, the longer the transition

time will be. Thusly, in applications where the prime power source is desired to be able to quickly start up and turn off, require either: fixing the ambient temperature around the fuel cell close to its operational temperature, another fuel cell type that has an operational temperature closer to the ambient, or the development of SOFC electrolytes that operate at closer to ambient rather than 500-1100 °C. Even the fuel cells with lower operational temperatures, 50-250 °C, require more time for initializing than other types of energy storage technologies [18]. While this can be accounted for in proactive load demand, in the case of an unexpected load demand, the retroactive response is slow.

Gao et al. [19] and Jones et al. [20] examined using fuel cells as the energy dense technology and batteries as the power dense technology in a HESM configuration. Since fuel cells can have significant start up and shut down times they need to be paired with an energy storage technology that can cover such times, which excludes many capacitors and makes batteries or flywheels the more attractive choice for pairing in a fuel cell HESM. The conclusions of both works is that for pulsed and military applications, the response time as well as the efficiency of fuel cells while idling are not good enough for use in a HESM at the present time and further research into fuel cell technology is advised.

2.3.3. Batteries

Of the aforementioned energy storage devices, batteries are attractive as the primary energy storage device due to their price, commercial availability, and ease of use. The high energy density reflects the large amount of energy that can be obtained from the electrochemical cells, and the low power density reflects the limit on how fast this energy can be provided to the load. The limitation on power density is a result of the time required for the electro-chemical reaction to occur and the exceptionally high internal equivalent series resistance (ESR) of the cells. A simple electrochemical cell is comprised of two half-cells. Each half cell contains an electrolyte with anions and the anode or an electrolyte with cations and the

cathode. The two half-cells are connected via an ion conducting electrolyte that also separates the other two ion charged electrolytes.

Of the different battery chemistries, two prevailing ones for usage in systems with pulsed loads are the lead-acid and lithium-ion chemistries. Connecting the cell's electrodes to an external charge or load circuit enables oxidation and reduction reactions to occur, creating an electrical current. When the cell is charged, electrons are extracted from the cathode and travel through the external circuit to the anode. During discharge in lead-acid batteries, positive hydrogen ions migrate out of the anode to the cathode. In conjunction with the hydrogen ion transport, sulfuric acid is consumed in reactions at both the anode and cathode. When a source is applied to the battery to recharge it, the reverse reactions occur. The reversible reactions for the cathode and anode are given in equations 2.1 and 2.2, respectively.

$$PbO_2(s) + HSO_4^-(aq) + 3H^+(aq) + 2_e^- \Leftrightarrow PbSO_4(s) + 2H_2O\ (I) \quad (2.1)$$

$$Pb(s) + HSO_4^-(aq) \Leftrightarrow PbSO_4(s) + H^+(aq) + 2_e^- \quad (2.2)$$

Similarly, for lithium-ion batteries during charging, lithium ions migrate out of the cathode, travel through the electrolyte, and collect in the porous graphite anode. This builds up a potential across the two electrodes and when the cell is disconnected from a charger and connected across a load, the reverse processes occur. The reversible reactions for the cathode and anode are given in equations 2.3 and 2.4 respectively. Figure 2.10 provides a visual diagram of the overall discharge reactions for both lead acid and lithium-ion batteries.

$$LiCoO_2 \Leftrightarrow Li_{1-x}CoO_2 + xLi^+ + xe^- \quad (2.3)$$

$$xLi^{t+} + xe^- + 6C \Leftrightarrow Li_xC_6 \quad (2.4)$$

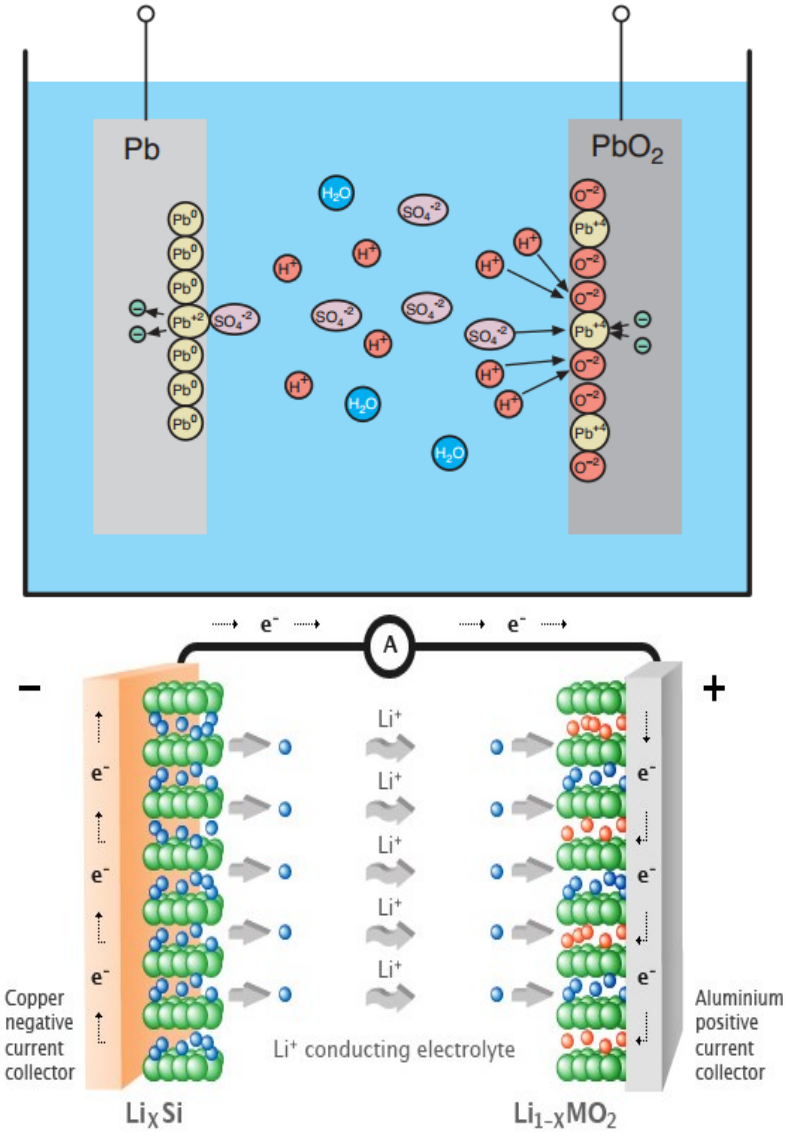

Figure 2.10 Battery Reactions: Lead-acid Battery (top) [21] and Lithium-ion battery (bottom) [22]

The lead-acid chemistry is less volatile and typically less costly than the lithium-ion but suffers from inferior power and energy densities with respect to both weight and volume. The safety concerns regarding the potential thermal runaway of lithium-ion batteries have been of concern both for commercial and research use, particularly for applications that operate energy

storage under more adverse conditions. Of the lithium-ion chemistries, lithium iron phosphate is one of the more popular due to improved stability over most other lithium-ion chemistries.

Research by Shrestha [23] and Novak [24] show that the repeated discharge and recharge of both lead-acid and lithium-ion cells at elevated C-rates drastically reduces the number of life cycles. The C-rate of an electrochemical cell is the current normalized by the 1 C-rating current. The 1 C-rating current is the number of Amps that can be continually discharged from a battery in one hour to discharge a fully charged battery. At elevated C-rates, the overall ESR of the electrochemical cells increases over time at a faster rate than at the rated C-rate, with respect to constant temperature. This growth in the ESR is a result of a combination of factors that includes but is not limited to: deposit buildup on the anion, depletion of charge carriers in the electrolyte, and development of gas bubbles within the electrolyte. To offset the effects of battery degradation on the load system, the batteries must either be frequently replaced which greatly increases maintenance costs, or the batteries must be paired with a power dense energy storage device that is setup to reduce the strain on the electrochemical cells.

2.3.4. Capacitors

The other type of energy storage seen in pulsed power research is the intermediate energy storage often made up of inductors and capacitors. These devices have high power density and low energy density and make a good match for pairing with batteries in a HESM. The compatibility of an inductor is primarily dependent upon physical geometry and core material. Inductors store energy in a magnetic field they seek to maintain a constant current through the windings to prevent changes in the magnetic field. To implement inductors as an energy storage technology within a HESM would require that the current loop that would maintain the stored energy in a fully energized inductor be lossless. The materials required to make a ‘lossless’ circuit loop for high currents are costly. Greater energy storage technology cross-compatibility can be achieved with batteries and capacitors that when fully energized can

be disconnected and store energy in an open circuit state. As a result, energy storage research with the inductor as a point of focus has been marginal.

Capacitors have significant research potential in the form of corrugated surface faces to increase surface area, employing various chemical properties as seen in fuel cells and batteries to further increase capacitance while minimizing the loss of power density. The incorporation of electro-chemical elements to improve energy density over purely physics based capacitance comes at a price of lower power density as could be seen previously in Figure 2.10. This hybrid type of capacitor is known as an electro-chemical capacitor or super-capacitor.

Two prevailing implementations of the super-capacitor arch-type are the Electric Double Layer Capacitor (EDLC) and the Li-ion Capacitor (LIC). EDLCs are a type of power and modestly energy dense capacitor. The electrodes are made up of metallic conductors that are coated with a porous activated carbon. The porousness provides an increase in the surface without increasing the physical dimensions. The two electrodes are separated by an aqueous, non-aqueous, or a solid polymer electrolyte. When a potential is applied across the electrodes, the ions within the electrolyte are polarized. This creates an alignment of opposing charges along the electrode/electrolyte interface. This alignment occurs for both plates and results in a Helmholtz double-layer of charges, from which the name is derived. The double layer formation of charge and the resulting voltage potentials throughout the capacitor are shown in Figure 2.11. Because the area of the electrodes is very large and the charge is separated by the extremely short distance of a few nanometers, the resulting capacitance of the cell can be extremely high (100 F/g^{-1}) [25]. The large electrode surface area coupled with their light weight (~800 m^2g^{-1}) [25] gives them their high energy density with respect to simple capacitors. However, because the charges are separated by such a small distance, the potential the cell is able to provide is small. The potential can be as high as 5V but is normally less than 3 V, in order to prevent electrical breakdown of the cell.

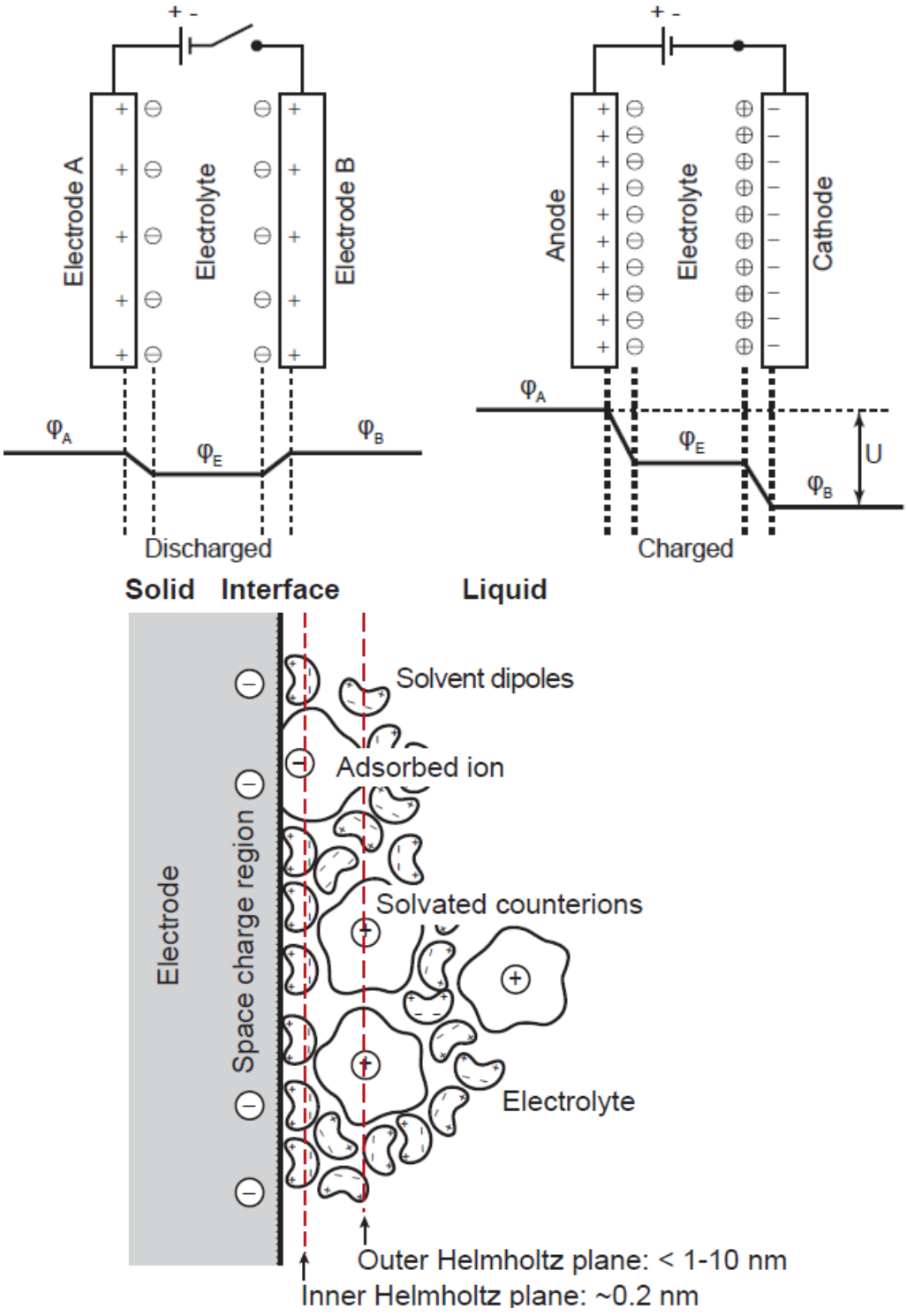

Figure 2.11 EDLC Operation: Images of the electric double layer [26]

By doping the anode of a super-capacitor with lithium, the anode capacity is increased. This causes the working voltage potential across the lithium-ion capacitor to be larger than a basic EDLC. The resulting voltage range is roughly 2.2 V to 3.8 V rather than 0 V to 3.8 V of an EDLC. The increase in working voltage gives lithium-ion capacitors a higher energy density than a basic EDLC [27]. However as a result of the non-zero minimum voltage, of lithium-ion capacitors is that like lithium-ion batteries, they should not be completely discharged otherwise the cells suffer significant and permanent capacity loss including total loss of functionality. Comparing the overall materials of a lithium-ion capacitor to both an EDLC and lithium-ion batteries yields the following relations: the anode is the same as that of the lithium-ion battery, and the cathode is the same as that of an EDLC electrode. A visualization of the comparison along with an illustration of charge storage is shown in Figure 2.12. The comparison of the resulting overall ESR of the super-capacitors is reflective of this electrode comparison. For large surface area cells the ESR of an EDLC is roughly 0.3 as opposed to the LIC with 0.8 mΩ. Due to the ESR the EDLC is capable of achieving a higher power density, however lithium-ion capacitor technology is newer and with further research its power density may overtake that of the basic EDLC. Because the cathode in lithium-ion capacitors does not include an oxygen compound, no thermal chain reaction or thermal runaway occurs as the cathode cannot react with the electrolyte [29]. None of the over-charge, over-discharge, over-heating, and nail punch tests performed by a lithium-ion capacitor manufacturer, JSR Micro Inc., resulted in thermal runaway of the cell [28].

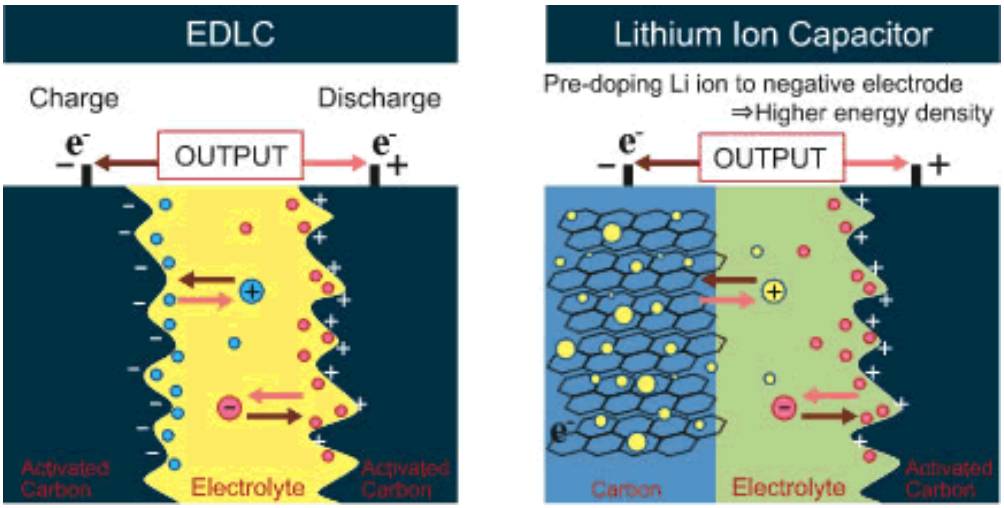

Figure 2.12 Visual comparisons of EDLC and LIC working principles [29].

Of the energy storage technologies, capacitors have among the highest power densities and lowest energy densities. Because of this when the energy storage is needed to operate for a period of time, capacitors are paired with another energy storage device type of a higher energy density. As a result, the super capacitors can be used as both a buffer for transient pulses in the load as well as peak shaving for those transients with respect to the batteries as demonstrated by Gao et al [11]. This hybrid pairing of different energy storage modules forms the basis of the HESM.

In the work presented by Gao et al. [11,19] the relationships between the system currents for long term operation was looked into. The result was that the battery output current must be the average of the HESM output current. The time averaged current provides the minimum current to sustain both the load and recharge the capacitor. The capacitor recharge maintains the bus voltage across pulsed load occurrences. Of note is that this battery output current is not the current that passes through the battery but rather the output current of the power electronics after the battery and can thusly be higher or lower than the actual battery current depending upon relative voltages in a particular HESM configuration. This experimental HESM validation employed a small number of energy storage devices. The battery bank was

composed of two units along with a single capacitor. The working voltages of these devices were less than 8 and 5 volts respectively and the max current in the HESM was 30 amps. Reasons behind such low system power in the verification of the time average current include the ratings for the inductors and capacitors, and that the power electronics were simulated using reconfigurable hardware-in-the-loop test equipment that has voltage and current limitations.

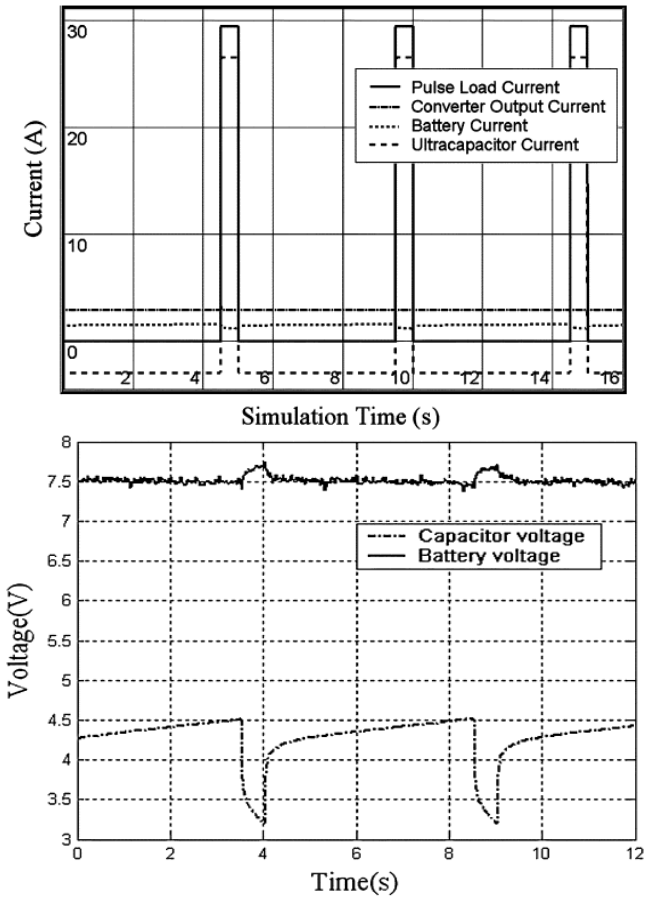

Figure 2.13 Time Average Current Experiment: Results from Gao et al. [11]

The importance of deploying HESMs in future naval ships has been shown. In addition, following government practice, these modules are to employ commercial products when possible. The products and technologies that comprise a HESM, both the energy storage and interconnecting electronics, have been compared and had their principles of operation as well as advantages and disadvantages explained. What will be shown next is the impact that pulsed

loads have on an isolated system's power quality and how a HESM employing COTS can be implemented to improve system response to pulsed loads. Included will be the original design principles of the COTS HESM as well as details regarding changes from the initial design to improve the capability and operational states of a COTS HESM. The effectiveness of COTS HESM will be analyzed. Overall design guidelines reviewed and summarized. Finally, the next steps of COTS HESM development and response to both pulsed and other load profiles will be envisioned.

Chapter 3

Experimental Setup

The testing of the impact of pulsed power loads on an isolated system architecture where the pulsed load power draw is significant compared to the size of the system was performed using the UTA MicroGrid Lab. This experiment sets the foundation for examining the effectiveness of a HESM to support high power pulsed or transient loads in an isolated electrical grid such as aboard an AES. First, the effects of the loads on a local electrical grid whose power generation is not oversized for the load demand will be examined on the basis of power quality analysis. From this, metrics for quick, efficient cross examination of power quality impact due to high power transient loads will be identified and subsequently used to analyze the experimental results when incorporating a HESM. The lab contains a MicroGrid test-bed that is comprised of three smaller microgrids that can be operated independently or collectively. Each microgrid has a 24 VDC bus as well as a 120VAC-60Hz AC bus. In the nominal configuration, two 12 VDC lead acid batteries are connected in series as the primary energy storage. The batteries on each grid are primarily recharged by renewable energy sources but can also be recharged by the electrical utility grid or a generator by employing the power transfer capabilities of the DC/AC inverter-charger. The renewables include dedicated solar panels and wind turbines for each MicroGrid, and, additionally, on “MicroGrid One” a PEM fuel cell is also installed. Each grid has its own DC/AC inverter-charger manufactured by Outback Power Systems. Also, each AC bus has a dedicated programmable load installed. However, the microgrids are not limited to only the programmable loads but can also drive conventional loads using standard US electrical power outlets. For the implementation of control over points of connection, each grid has Crydom solid-state relays installed at the various points of connection on the AC bus. For

control of the DC bus contact switches are employed. The control of connections is performed using a National Instruments CompactRIO control system. A block diagram overview of the current setup including devices used is shown in Figure 3.1.

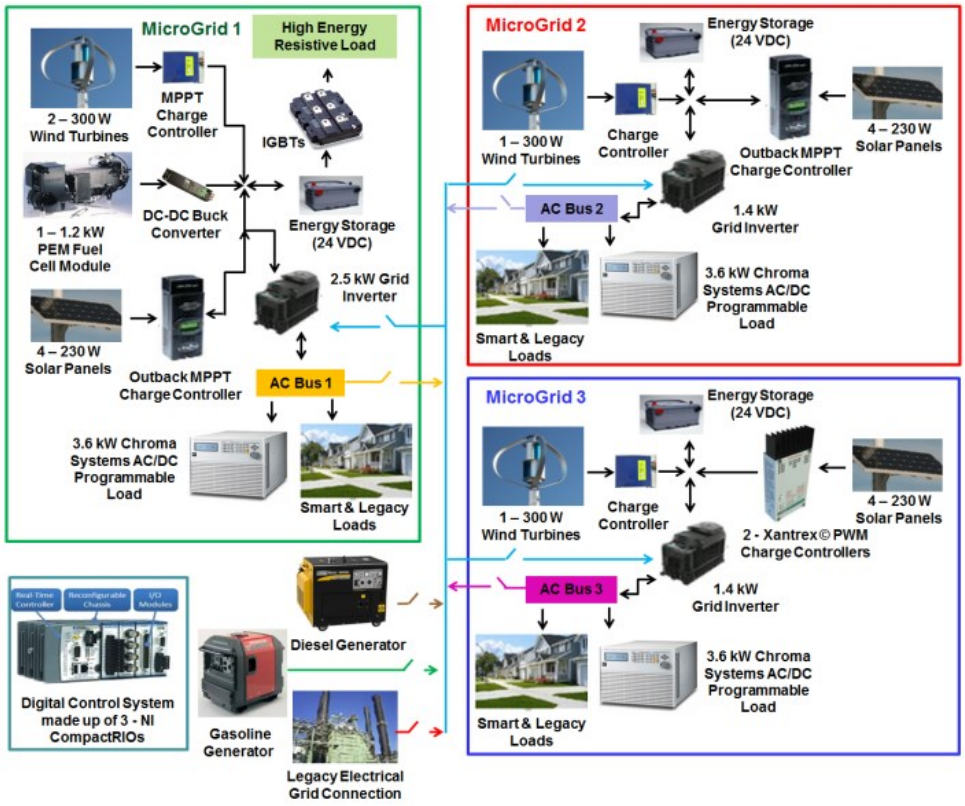

Figure 3.1 UTA MicroGrid: Comprises three independent microgrids which can operate independently or in an interconnected fashion.

Each of the three microgrids has its own distributed energy sources (DESs), dynamically reconfigurable real-time control system, and dedicated loads. This enables each of the microgrids to function as its own independent electrical grid in the normal mode of operation and also enables each of the microgrids to source another's loads, via a central AC bus. This architecture was chosen for a couple of reasons. First, the DoE's Smart Grid concept involves the communication and interconnection of several independent MicroGrids, what could be called Smart nodes, to increase system reliability, efficiency, and robustness. Second, the

Department of Defense's (DoD's) planned zonal electrical architectures involve the communication of several different DESs configured in various smaller grid configurations throughout the platform, AES, or base installation, FOB [30]. Therefore, the current UTA configuration supports both of these agencies' missions.

The UTA MicroGrid incorporates several different renewable energy sources along with a conventional diesel generator and the legacy electrical grid to power the test-bed loads. Each of the three sub-microgrids harnesses wind energy through the installation of DS300 HiVAWT vertical axis wind turbines [31] and solar energy via, ~30 V, 230 W Schott solar panels [32]. A total of 1.2 kW of wind turbines and 2.76 kW of solar panels are installed. Each of the three microgrids has four solar panels installed that are connected in a 2 series / 2 parallel configuration. The solar panels installed on MicroGrids One and Three are each fed into its own grid dedicated FLEXmax 60 maximum-power-point-tracking (MPPT) charge controller manufactured by Outback Power Systems [33]. Each of the series stacked solar panels connected on MicroGrid two is fed into its own Xantrex C40 pulse width modulated (PWM) charge controller [34]. The different charge controllers were chosen so that researchers and students could compare the difference between the MPPT and PWM charging technologies. Each of the 300 W wind turbines is tied directly into its own 400 W MPPT charge controller manufactured by HiVAWT. Of the four vertical axis wind turbines, two are dedicated to MicroGrid One, and MicroGrids Two and Three each have a single dedicated wind turbine

In addition to the renewable DESs discussed above, MicroGrid one has a NEXA 1.2 kW proton exchange membrane (PEM) fuel cell manufactured by Ballard Power Systems [35] installed. The working voltage of the fuel cell starts out at 45 V and decreases down to 26 V as the output power approaches 1.2 kW. A 5 kW DC-DC buck converter, model CH100105F-S, developed by Zahn Electronics conditions the fuel cell's unregulated power and ties it into the grid's DC bus [36]. Each microgrid has two series connected 12 V – 1150 CCA DieHard® Platinum gel-cell batteries for energy storage [37]. The equivalent series impedance of the gel-

cell batteries are 4.2 mΩ while that of the power converter it is connected to is 3.2 mΩ in charging mode. The regulated DC output voltage from each charge controller has an output point of common coupling with the batteries which provide energy when the AC utility grid is unavailable or the cost of utility power is above an acceptable value. While gel-cell batteries are currently installed, future plans include installing other forms of electrochemical energy storage, such as lithium-ion batteries, lithium-ion capacitors, and super capacitors in order to understand the benefits these new technologies offer for driving both conventional and high power Smart loads.

The 24 VDC bus on each of the microgrids connects directly to a dedicated DC/AC sine wave grid-tie inverter manufactured by Outback Power Systems. A GTFX1424 [38], 1400 W inverter is installed on MicroGrids Two and Three while a GTFX2524 [39] 2500 W inverter is installed on MicroGrid One, due to the higher input power available from the additional renewable sources. Each inverter-charger can operate in an islanded or grid-tied mode of operation and outputs a 60 Hz, single phase, 120 VAC filtered sine wave. Each output of the inverters first passes through a no-fuse-breaker (NFB) which will that automatically open in an overcurrent event for safety. Subsequently, the current feeds into a digitally controlled solid state relay (SSR) [40]. These relays are used to isolate and protect the MicroGrid system devices in cases where a critical overvoltage or overcurrent condition is detected by the real time control system. Finally, the output of the SSR is connected to the microgrid's central AC bus.

Each grid has dedicated loads connected to its respective central AC bus via a series connection of a NFB and a SSR to ensure safety, controllability, reliability, and flexibility. A 3.6 kW, AC/DC, 63803 programmable load manufactured by Chroma Systems [41] exists on each grid as a means to simulate a realistic load profile including the implementation of transient load conditions. In addition to the programmable loads, conventional loads such as light bulbs, fans, etc. can also be installed on each grid and controlled using the load's dedicated SSR. The

digital controllability enables researchers to develop and test load shedding algorithms which ensure that the most critical loads will have power in the event of an energy shortage.

In the normal mode of operation, the inverters operate in a grid-tied fashion, connected to a central AC bus, using the legacy electrical grid as a reference. This mode of operation allows the inverters to use the legacy grid to power loads and charge energy storage devices. Also, the energy storage can be used to serve the loads, mitigate the intermittence of renewable resource, and provide ancillary services to the grid. In the event of a legacy grid outage or other isolation event, the inverters will automatically convert over to an off-grid, island, configuration, using the batteries to source the loads. If any particular grid's energy storage runs low and critical loads are still in need of power, the AC output bus from any of the other microgrids can connect to the central AC bus and source power to the grid(s) in need.

Finally, in addition to all of the renewable DESs already mentioned, two fossil fuel power generators are also installed. The first is a DuroStar DS7200Q, 6 kW diesel generator, and the second is a Honda EU3000is, 3 kW gasoline generator [42, 43]. Originally only the Durostar was used but was found that under light load conditions, such as when only one or two of the microgrids were connected, the output frequency would have a deviation beyond what the Outback power converters would accept, so a second smaller generator with tighter regulation on voltage and frequency output was acquired for use below the 3 kW range. If the energy from the legacy grid is too expensive or otherwise unavailable and the energy storage runs low, the generator can source the AC input of the microgrid's inverter via the connection to the central AC bus. The name, quantity, and power output specification of each DES are listed in Table 3.1 and that of the different charge controllers are found in Table 3.2. Photographs of various portions of the full MicroGrid test-bed are shown in 3.2 through Figure 3.7.

Table 3.1 Distributed Energy Sources (DES) Specifications

Device	Quantity	Individual Power Rating (W)
HiVAWT DS-300W Wind Turbine [32]	4	300
Schott Poly 230 Solar Panel [33]	12	230
NEXA™ 310-0027 Ballard® PEM Fuel Cell [36]	1	1200
DuroStar DS7200Q Diesel Generator [43]	1	6,000
Honda EU3000is Gasoline Generator	1	3000
DiHard®1150 CCA Platinum gel-cell batteries	6	13,800 (CC)

Table 3.2 Charge Controller and Inverter Specifications

Device	Quantity	Power Rating at 24V DC (W)
HiVAWT WT23000 MPPT Controller [32]	4	384
Outback Power FLEXmax60 MPPT Controller [34]	2	1800
Xantrex C40 PWM Charge Controller [35]	2	960
Zahn Inc. CH100105F-S Buck Converter [37]	1	2520
Outback Power GTFX1424 Sine-wave Inverter [39]	2	1400
Outback Power GTFX2524 Sine-wave Inverter [40]	1	2500

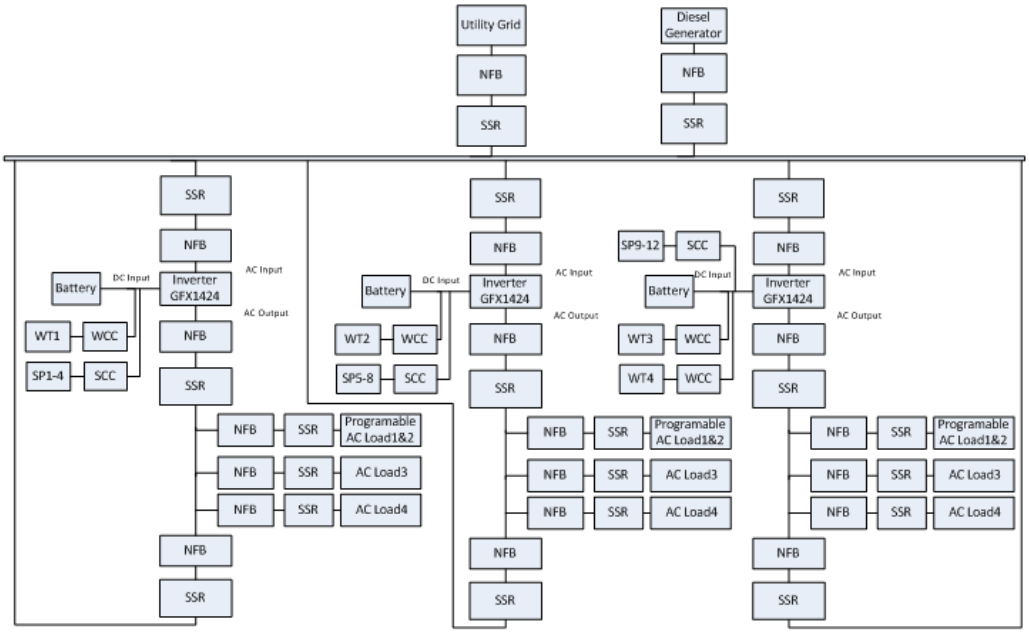

Figure 3.2 UTA MicroGrid Relay & Switch Schematic.

Figure 3.3 UTA MicroGrid Renewable Installation: Photograph of the solar panels, wind turbines, and diesel generator (under solar panels) on the roof of UTA's Engineering Laboratory Building.

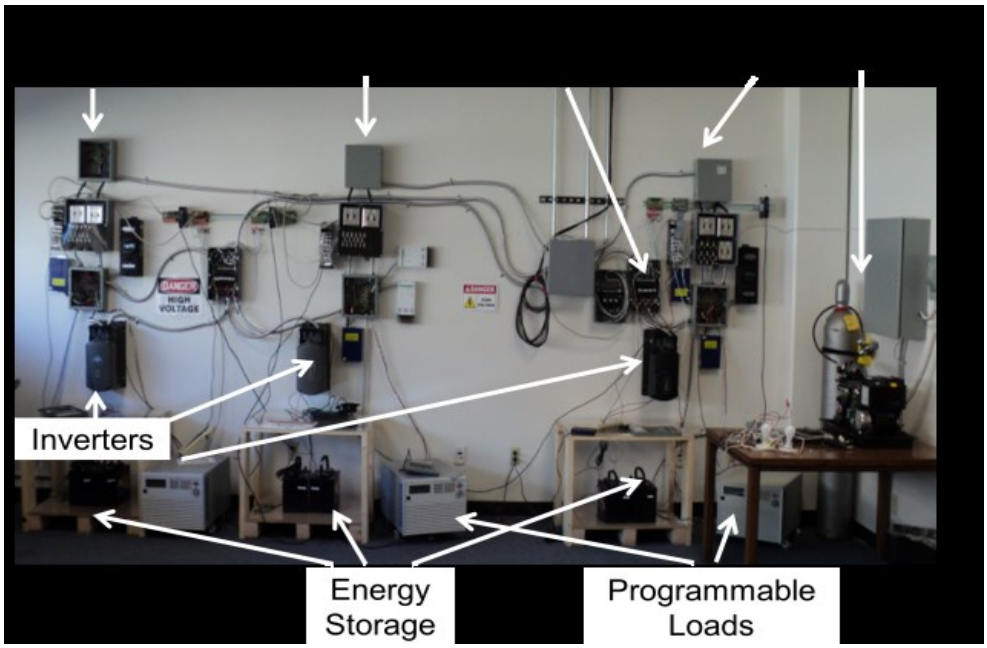

Figure 3.4 UTA MicroGrid Image of laboratory.

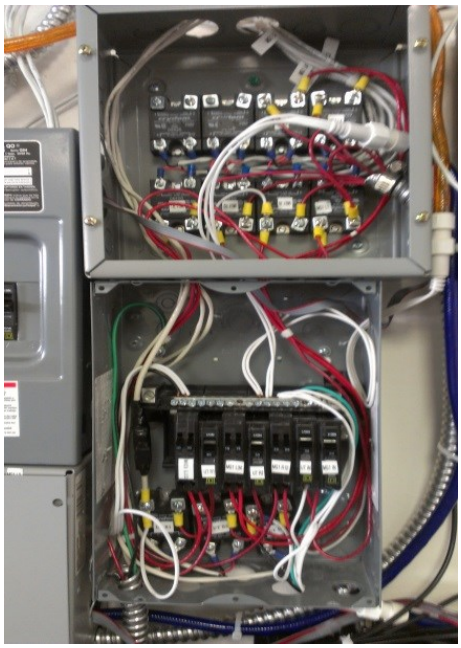

Figure 3.5 UTA MicroGrid 1 Bus Image: Close-up photograph of the NFB and SSR relays used to regulate the flow of power from the legacy electrical grid and MicroGrid 1

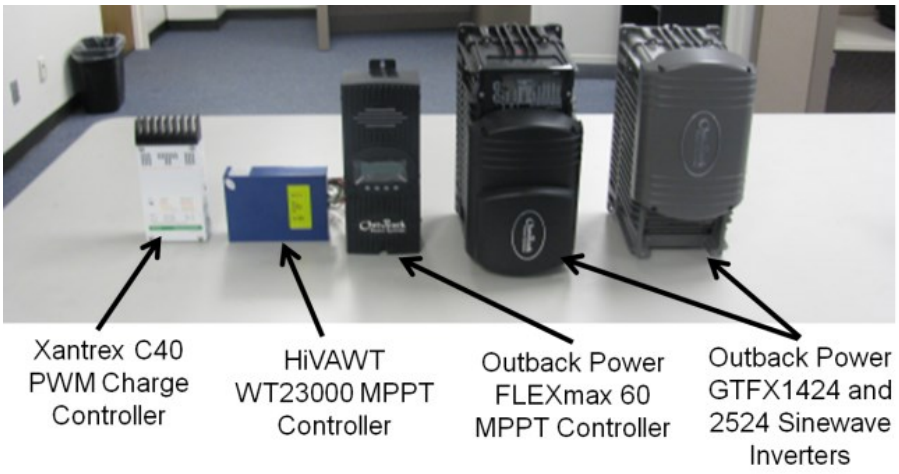

Figure 3.6 UTA MicroGrid Power Electronics: Photograph of the charge controllers and sine-wave inverters.

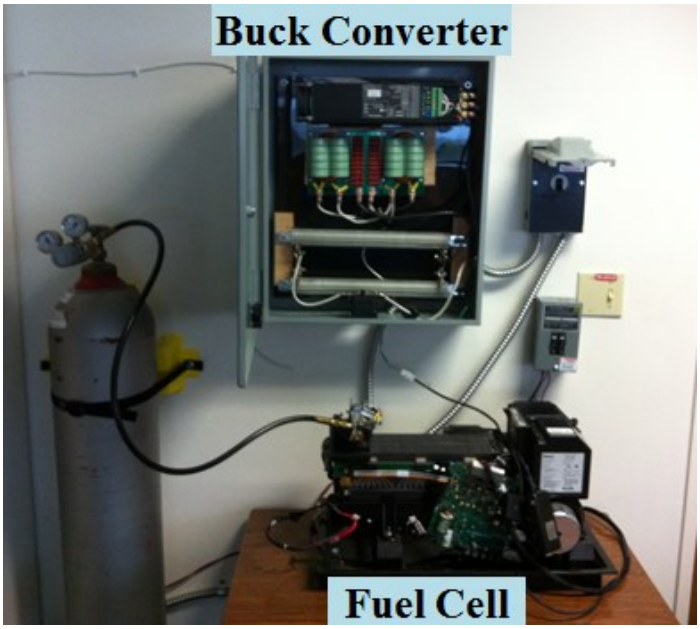

Figure 3.7 UTA MicroGrid Fuel Cell: NEXATM 310-0027 Ballard® 1.2 kW PEM Fuel Cell [36]

The microgrids have four load lines apiece, each of which is connected to the AC bus via its own NFB and SSR for safety and independent controllability. Originally, the first two load lines of each grid were connected in parallel to a Chroma model 63803 programmable AC/DC

Load. The reason behind this is the SSRs had a 25 A rating and the max current draw of the programmable load is 36 A. For medium and low power draws by the programmable load no issues were detected. Under ideal or simulation conditions the same model SSRs obtained at the same time should have split the current to the load for the higher load current draws. However, this was not the case. The small internal differences among the SSRs, even those of the same batch, would result in one carrying all, or the vast majority, of the current resulting in only one of the two NFB paths also carrying the current as each SSR is directly connected to a single NFB. This caused a buildup of electrical action in the NFB and resulted in one NFB tripping after a duration of high load usage. Subsequently, all the current would then be dumped down the other path and cause the other NFB to trip as well. To correct for this issue the SSR was replaced by its 90 A variant and the NFBs were upgraded from 15 to 25 A ratings. Due to space limitations higher rating NFBs, could not be readily implemented, therefore the single 90 A SSR feeds two 25 A NFBs in parallel.

A programmable load is a type of load that can change its operating mode and parameters on the fly. These modes of operation include: constant current, constant resistance, constant voltage, constant power, and rectified load. It can dissipate 3.6 kW with a peak operating voltage of 350 V_{RMS} and current of 108 A_{peak} / 36A_{RMS}. The programmable load will be used to provide baseline loading as well as applying load profiles and inducing transient load conditions onto the microgrid. The other two load lines on each grid are currently configured to power conventional 120 VAC, 60 Hz loads via a standard US plug connection. In the future, it is hoped that more Smart loads capable of representing a wider range of load profiles with improved response times will be developed commercially and installed on the MicroGrid.

In addition to conventional AC loads, the microgrids are configured to test how transient DC loads and faults impact the quality of the voltage on the main AC bus. This is accomplished by connecting two ABB HiPak 5SNA 2400E170100 Insulated-Gate-Bipolar-Junction (IGBT) transistors [44] in anti-series with each of the three IGBTs per housing connected in parallel.

The total IGBT configuration is connected between the DC energy storage and a high power adjustable impedance load. Each switch can hold off 1.7 kV, conduct 2.4 kA continuously, as long as the collector temperature stays below 80^{o}C, and can conduct a peak surge current of 20 kA for roughly 10 ms. Initially, a low impedance load that is almost purely resistive is being used. A series/parallel connection of up to 20 – 100 mΩ high energy disk resistors enable the load to vary easily from roughly 8 mΩ up to 2 Ohms. The dynamic Chroma programmable loads could not be used for a pulsed load due to the roughly one second delay response in changing load operation mode upon receiving the command to do so.

For controllability, each microgrid has its own real-time digital acquisition and reconfigurable embedded control system, National Instruments (NI) CompactRIO, installed as seen in Figure. The CompactRIO's hardware architecture incorporates a reconfigurable field-programmable gate array (FPGA) chassis, an embedded controller, and the ability to easily swap out different I/O modules as needed [45]. The system's programmed using NI's LabVIEW graphical programming tools and can be used in a variety of embedded control and monitoring applications. Each grid's CompactRIO has eight I/O modules installed that give it digital output, digital input, analog output, and analog input capability. The digital and analog output signals are primarily used for relay and device control. The digital and analog input channels are used for real-time monitoring, data collection, and feedback control.

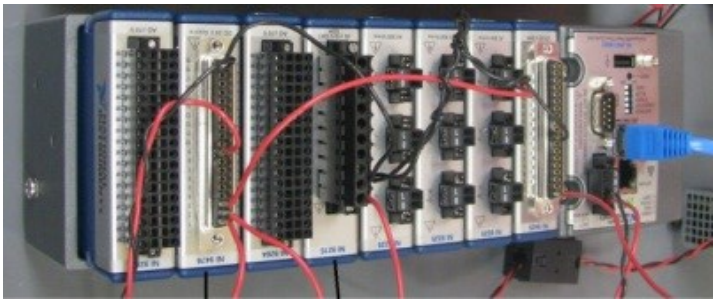

Figure 3.8 National Instruments CompactRIO data acquisition and digital control system.

Each CompactRIO can be controlled using a single, remotely accessible, visual user interface (VI) programmed into and ran directly from the CompactRIO. A regular computer is

used as a host machine for passing data between the three microgrids. The voltage and current at nearly every input and output in each of the different microgrids is monitored using voltage probes and Hall effect current sensors whose outputs are fed directly to the analog input channels on each MicroGrid's respective control system. In response to changes detected through the sensors, the LabVIEW VI uses the CompactRIO's digital outputs to control the various SSRs. Since each of the components connect to their respective grid through a dedicated SSR, they can be disconnected from the grid quickly when any unstable operation is detected or the need for a load shedding condition arises. The components are just as quickly able to return to the grid when a desired state of operation occurs. This capability gives the grid a self-healing capability. The name, quantity, and specifications of all the hardware that makes up each microgrid's CompactRIO is listed subsequently in Table 3.3.

Table 3.3 UTA MicroGrid NI CompactRIO Specifications: Data acquisition and control system (all components listed are installed on each grid)

Device	Quantity	Specifications
CRIO-9114 Reconfigurable CompactRIO Chassis	1	8-slot, Xilinx Virtex-5 reconfigurable I/O (RIO) FPGA core
CRIO-9022 CompactRIO Real-time Controller	1	533 MHz, 2 GB storage, 256 MB DRAM
NI 9476 Sourcing Digital Output Module	1	32-Channel, 24 V, 2 kHz
NI 9425 Sinking Digital Input Module	1	32-Channel, 24 V, 140 kHz
NI 9264 Analog Output Module	1	16-Channel, ±10 V, 25 kS/s, 16-Bit,
NI 9215 Simultaneous Sampling Differential Analog Input Module	2	4-Channel, 16-Bit, ±10 V, 100 kS/s/Ch
NI 9225 Simultaneous Sampling Differential Analog Input Module	3	3-Channel, 24-Bit, +/-300V, 50 kS/s/Ch

3.1 Power Quality Impact Experimental Setup

For the experimental testing of the impact of pulsed loads on the power quality of an isolated electrical system where the pulsed load power is significant compared to the power capabilities of the electrical grid, only MicroGrid One was used. This microgrid contains greater total power generation and subsequently higher rating power electronics than the second and third grids. A more detailed configuration of MicroGrid One can be seen in Figure 3.9 below.

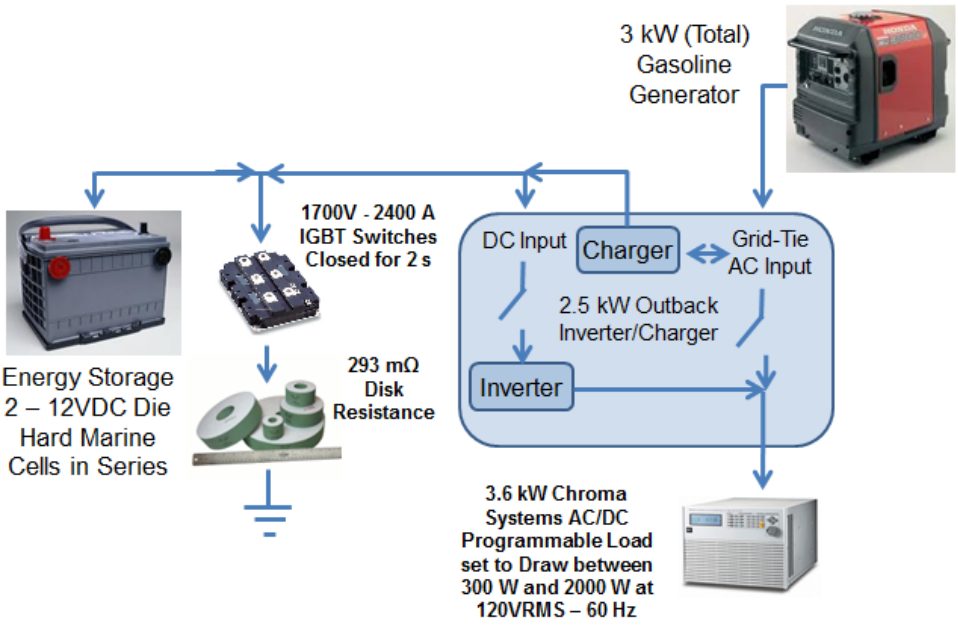

Figure 3.9 UTA MicroGrid 1 Power Quality Setup: Section of the MicroGrid being used in the research presented here. (Note the Outback inverter schematic has been greatly simplified for presentation and is not representative of all the internal workings)

In the pulsed load experiment for power quality, the solar panels, wind turbines, and the PEM fuel cell have been left disconnected from the grid to focus the analysis on the energy storage and provide the ability to accurately correlate the improvement or possible lack thereof. The pulsed load is connected in parallel with the energy storage and the DC connections of the DC/AC power converter. The pulsed load is comprised of a series combination of disk resistors that for the experiments were configured to form a 293 mΩ load. This value for the pulsed load was chosen so that roughly 80A of peak DC current would be drawn from the system. The connected or disconnected states of the pulsed load are controlled by the NI CompactRIO and implemented utilizing the IGBTs.

It was intended that the inverter would continuously monitor the energy storage voltage. So long as the energy storage voltage was above the minimum threshold of the Outback power converter, energy would be sourced from the energy storage, through the inverter, and to the

programmable load. Whenever the voltage dropped below the threshold, which will occur when the DC load is pulsed with high current for a few seconds, the inverter would kick into grid-tie mode where it passes through energy from the diesel generator to the AC load and also turns on the battery charger to 'recharge' the DC bus. Once this occurred, it was hoped that the energy storage and the charger from the batteries would both be sourcing current to the low impedance disk resistance. Instead, one of two things happened. Firstly, the power converter did not kick in the generator pass through and instead allowed the energy storage to continue sourcing the AC load while it also sources the DC disk resistor load. This causes the conduction voltage of the energy storage to drop below the inverter's minimum input voltage which subsequently causes the AC output voltage to drop significantly below 120VAC – RMS. Secondly, the power converter did not pass through the generator continuously even during non-pulsed load operation. It was found that the energy storage should only have been used when the power converter senses issues with the generator power quality according to the power converter's programming at the time. The result was the occasional cut out of pass through randomly for a few seconds at a time.

Regarding the first issue, it was discovered from the manufacturer that the inverter is designed to only poll the input battery voltage every few minutes. This few minute delay in the design of the power converters is based on expected operation conditions for residential usage where the delay to a change in the state of the DC bus is not desired to be fast. The AC input's voltage and frequency are calculated at a much faster rate but have programmed in delays before responding to drastic changes in operating conditions. Therefore, when the DC load is pulsed and causes the battery voltage to drop below the threshold, the Outback power converter misses it completely in most cases and continues what it was doing before. Additionally, if sequential polling events occur during separate pulsed load events, the power converter may change from inverting to charging during a third or later pulsed load test resulting in the false

appearance of expected operation in the later test. Overall, this behavior of the power converter resulted in inconsistent system operation for subsequent and repeated tests.

To correct for this issue, several initial conditions for the experiment are placed under tighter control. Because of the long transition time to alternate between inverting and charging, or visa-versa, the experiments will focus on the energy storage in combination with the primary power of the DES to provide power to the pulsed load, with the DES also supplying the local AC load. This scenario calls for setting the Outback power converter in charger mode with respect to the DC bus. As none of the preprogrammed AC power converter operation modes affected the response time of the DC bus within the timescale of the pulsed load profile, all AC operation modes were disabled. However, basic AC mode functionalities, such as generator connect & disconnect as well as AC load connect & disconnect based upon voltage and frequency conditions, were set to be operational. It is expected that enough of a change in power flow at near max conditions should produce some noticeable changes on the power quality on both the AC bus connected to the generator and the AC bus connected to the load. If the drop is significant, the power converter may kick off the AC input due to the drop below acceptable AC voltage input. In order to work around the DC bus polling and ensure consistency across tests, the COTS power converter was reset between tests.

Regarding the second issue, on the seemingly random generator-converter disconnects, an experiment was performed using a load profile via the programmable load. The programmable load profile was set to draw constant power, stepping up from 500W to 1.8 kW. Analysis of the test for generator bus voltage showed the frequency output of the DuroStar diesel generator was unable to maintain a frequency under 60.9 Hz. The maximum acceptable frequency of the Outback power converter is 60.8 Hz. Therefore, it will never maintain the conditions needed for pass through to the AC load or send power to the DC bus through the charger. This revealed the source of the second issue. Through communication with Outback Power Electronics, it was found that the Honda EU series of generators had been tested by

Outback and found to provide power quality that would meet the requirements of the power converter. A Honda EU3000is gasoline generator was obtained and setup as an alternative DES to the Durostar DSQ6000 diesel generator. During testing of the capabilities of the new DES, it was found to maintain 59.9 Hz under full load conditions.

The procedural steps for the system setup prior to each experiment are as follows. The gasoline generator is checked for fuel status and full electrical output is confirmed as operational. The programmable load is set to draw the desired constant power load at 120 VAC and 60 Hz. The DC/AC inverter is set to pass through the generator input to the Outback power converter's AC output and the connected programmable load. The power converter's DC charger is manually set on so that current is initially flowing into the batteries. On the DC side, the charger is capable of sourcing up to 55 A RMS and does so in a 120 Hz pulsed fashion with duty cycle of 50%. The sinusoidal form of the DC current is a result of output filters and the on-off states of the converting operation.

This setup was chosen to experimentally determine the impact on power quality during the operation of a high DC pulsed load and high power AC load simultaneously. Three sets of experiments were performed. Each set of experiments tested the system through a range of eighteen constant power programmable load values. The programmable load was set to draw 300 W initially, with that value being incremented by 100 W in each subsequent test, up to 2000 W. Initially, the pulsed load was inactive for the recording of the initial steady state conditions for a particular AC load. The pulsed load would then be activated by the IGBTs and follow a pulsed load profile set within and controlled by the CompactRIO. Three different pulsed load profiles were run. The first profile consisted of a single two second long, 100% duty cycle pulse. The second and third profiles maintain roughly the same total energy consumption as the first profile by keeping the total pulsed load on time as two seconds. These profiles are different in that they are 50% duty cycle for a total of four seconds. Where these two differ from each other is in their periods. The second profile has a period of 30 ms or 15 ms active, and the third profile has a

400 ms period or 200 ms active. The reconfigurable disk resistor pulsed load remained the same across all tests.

After the starting delay to obtain the initial system conditions with only the AC load, the IGBTs are closed connecting the DC bus to the pulsed load. The AC load remains constant throughout the test and the IGBT switching behavior follows the profile setup in the CompactRIO. After the pulsed load profile is finished, data recording continues for a few more seconds to obtain the system recovery response. Between tests, the energy storage was recharged and system components left to cool until back at room temperature.

The analysis of the above experiments will focus on the performance of a microgrid by its ability to source quality power to connected loads within the standards set out by defined specifications, such as MIL-STD-1399-300B, and IEEE-STD-519. In each of these standards, regulations are given which specify the allowable variance in the voltage, current, and frequency. The experiments will be evaluated in accordance with these standards on both the generator and load AC buses. As a result of the experiments performed here, metrics for both AC and DC system values will be obtained allowing for efficient power quality comparisons of the effects of different energy storage setups including hybrid energy storage modules in an isolated electrical grid with loading comparable to the power generation.

3.2 Experimental Setup for Evaluating a COTS HESM on Power Quality

With the increasing desire for further implementation of energy storage combinations in recent years both experimental research and the development of common standards for HESMs are needed. For the testing of performance gains of different energy storage technologies and renewable energy sources interconnected on an isolated electrical grid by looking at cycle life, power quality and pulsed power capabilities amongst other metrics, a HESM using COTS products was constructed. The usage of COTS components and in particular the power electronics minimizes the time spent on HESM development and implementation which allows for ease of experimental replication by end users or other

researchers. It also shifts the focus of the work to the operation and evaluation of different energy storage technologies for pulsed power applications. A high level electrical diagram of the COTS HESM experimental setup is shown schematically in Figure 3.10 and a photograph of the HESM in Figure 3.11

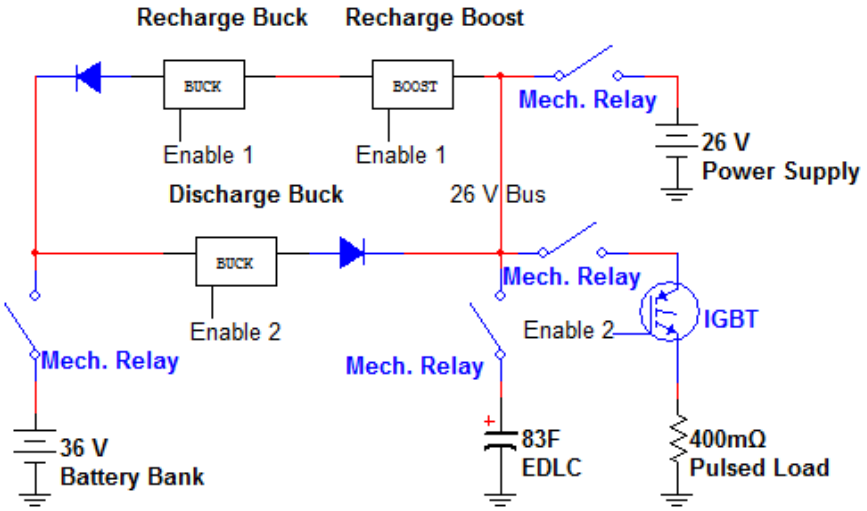

Figure 3.10 COTS HESM Circuit Diagram of active control.

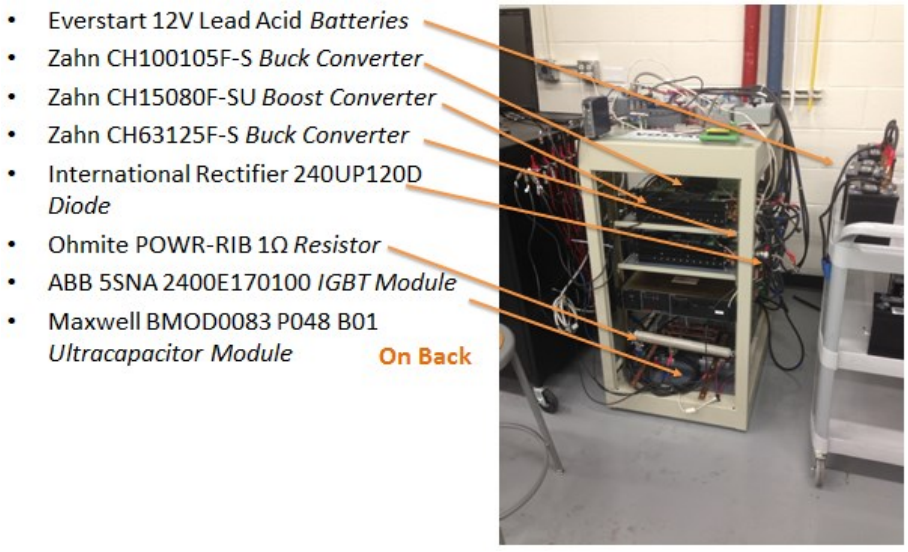

Figure 3.11 COTS HESM Physical Setup: Active Hybrid Energy Storage Control (middle), Monitoring Setup (left), Battery Bank (right)

For the research presented here the HESM has been configured using a 36 VDC battery module, a 48 VDC Maxwell EDLC module, a 40 VDC – 75 ADC grid tied power supply, two buck converters, one boost converter, two diodes, an IGBT-controlled load, and a National Instruments (NI) CompactRIO control system. The energy storage setup presented here employs three, 6 cell, lead acid batteries connected in series. These lead acid chemistry batteries were chosen as the primary energy storage to validate the base system metrics as a result of their low cost, ease of implementation, high durability, and relative safety. The output of the batteries is fed into two parallel paths made up of power electronic converters.

When the battery is discharging current to the load, the lower buck converter in Figure 3.10, which is a CH63125F-S manufactured by Zahn electronics, is used. This converter has an operational input voltage of 12 – 63 VDC, a maximum continuous current of 125 ADC, and operates with a switching frequency of 31.25 kHz. These properties, coupled with the ability to operate in a voltage controlled mode with adjustable current limiting make it ideal for this application. As will be shown later, the setup initially utilizes this converter with a 26 VDC output voltage and current limit of 20 ADC. This enables the battery bank to act as a DES for the HESM and to source the energy at levels for which the bank is rated for mostly independent of the demand from the load. The converter's current limit is dynamically adjustable by the control system. It is important to keep in mind that the buck converter steps down the voltage while maintaining as much of the power converted as possible. Of note when using COTS power electronics is differences in desired controls between manufacture and end use. An example is the current limit. The buck converters used have a current limit on the output and not the input. This means that setting the controllable current limit of 20 ADC on the buck converter does not result in the desired battery current of 20 ADC for the purpose of preserving battery life cycles. This requires the NI controller to adjust the output current limit to a value that achieves the desired battery current limit utilizing feedback control. The COTS converters used also have

output regulation control via an enable/disable control pin that will cause the buck and boost converters to cease their respective operation. The COTS buck converters used disconnect the input and output which causes the output side of the converter to be coupled to the common DC bus or PoCC during the recharge state. The boost converter maintains a connection between the input and output, dropping the voltage difference between the higher output voltage and lower input voltage across an internal diode. When 0 VDC is fed from the control system to the enable pin of a converter, the converter operates. When 5 VDC is applied to the enable pin of a converter, its output is inhibited, but current will still be allowed to flow backward into the converter, therefore a diode was placed on the output to prevent such a case. The boost converter can work with inverted logic polarity, so care must be taken when interconnecting logic controls of different COTS components for simultaneous control. All of the enable trigger pins operate on the order of ~5 ms. The advantage of using the enable/disable feature of the converter as opposed to an external switch is the avoidance of potential issues that arise in the internal operations of the converter from abrupt open circuits on the input or output of the converter.

On the central DC bus, the IGBT-controlled resistive load, the EDLC module, and a grid connected DC power supply are installed. Initially, the load is an adjustable, 1 Ω, Ohmite Powr-RIB® resistor. In the work presented here, the resistance has been adjusted to ~0.4 Ω. Two 2400 ADC IGBT's, ABB model 5SNA2400E170100, are used to connect the 'pulsed' resistive load to the DC bus. The three IGBTs of each module are connected in parallel and the two modules are connected in anti-series. Accounting for the small conduction voltage drop of ~2 VDC across the IGBTs, the resulting load requires roughly 60 ADC to be sourced to it when the bus voltage is maintained at 26 VDC. The IGBTs are controlled digitally by the NI control system using active high controls.

The power supply is installed to mimic a fossil fuel generator, after AC to DC conversion, which may be installed in a Navy FOB or shipboard installation. These types of

generators have an optimum operational condition at which they are most efficient. Therefore, it is best to operate them at this level and have them fluctuate as little as possible. This means that they should supply some base power to the load. The alternative sources, the batteries and EDLC in this case, should supply the excess transient and steady state power demanded by the load. In the event that the load is non-active, the energy storage should be used as an energy sink allowing the generator to continue operation at its most efficient level. This is of course beneficial to the energy storage as it gets recharged for future operation. In the setup here, the Sorensen DCS40-75E 40 VDC – 75 ADC power supply was used to mimic the effects of a fossil fuel based generator after AC/DC conversion, such as the gasoline generator connected to the Outback power converter of the pulsed load power quality experiment. For the following experiments, the power supply was internally limited with voltage and current limits of 26 VDC and 25 ADC, respectively, this follows the output current limit of the Outback power converter itself and in conjunction with the current that it had to prioritize in providing to the AC load over the DC charger. These values are also dynamically adjustable using the NI control system.

The EDLC is the only unregulated source in the HESM. The EDLC used for the results presented here is a Maxwell BoostCap Module with a capacitance of 83 F and a voltage range of 0 - 48 VDC. The EDLC is the most power dense source used within this COTS HESM and offers the ability to source high power with nearly no impact to its life. Therefore when 60 ADC is demanded from the HESM, 20 ADC are supplied from the battery, 25 ADC are supplied by the power supply, and the rest comes from the EDLC. Initially the EDLC should supply a higher front end power in response to the load as the response time of the power electronic converters have logic delays in their regulated power paths.

As previously mentioned, the DC power supply maintains its output power when the load is not sourced, instead supplying energy to recharge the EDLC and battery. Though batteries can be discharged at high rates with moderate impact to their cycle life, recharge at high rates can be very damaging and sometimes catastrophic. For that reason, a series

configuration of a boost and then buck converter are connected between the power supply and the batteries for battery recharge. This configuration is used since current limiting is not available from the COTS boost converter used. The boost converter, a Zahn CH15080F-SU, steps up the power supply voltage to 50 VDC and feeds it to the buck converter, a Zahn model CH100105F-S. The buck converter then steps down the boost output to a battery recharge voltage of 40 VDC and a current limitation of 7.5 ADC is enforced on the converter. The total capabilities of the boost converter are as follows: The input range is 80 - 118 VDC with an output range of +2 VDC of the set input voltage up to 120 VDC. The maximum input current is 80 ADC and output current 78 ADC. The buck converter has an input voltage range of 24 - 80 VDC and an output range of 0 - 79 VDC. The maximum continuous output current is 105 ADC. Both converters, like the buck described earlier have a switching frequency of 31250 Hz. The boost converter is enabled in the same manner as the discharge buck converter discussed earlier. The boost converter, when disabled becomes a voltage pass-through. Therefore, another diode is connected to the output of the recharge converter to ensure the batteries cannot back feed through this path during discharge of the circuit. Since the current to the batteries is limited, any excess current from the power supply is fed to the EDLC, restoring energy for the next connection of the load.

In order to effectively implement active control of the HESM components described above, a priority hierarchy for both active-load operation and inactive-load operation had to be implemented. The first priority during active-load operation is supplying the pulsed power load for which the HESM was implemented to primarily support. This includes not only supplying the current required by the load, but also maintaining the bus voltage within the range of the system requirements. The second priority is to maintain the maximum efficiency of generator operation. In other words, the HESM should be able to compensate for the load demands in excess of the generator's optimal power output. In order to accomplish this, the third priority must also be taken into account, which is to limit the current through the battery to minimize life-cycle loss.

By sizing the HESM components and controlling the power flow, it is possible to augment the generator while fulfilling all of these priorities.

In this configuration, the EDLC is the dominant voltage source on the DC load bus, sourcing transients when the load exceeds the limits applied to the batteries or power supply. Since the batteries and the power supply have current limitations enforced upon them, their voltages can sag when the load demands more current than they are able to supply. The voltage of the EDLC is determined by the energy it has stored, therefore the DC bus voltage directly correlates with the amount of energy sourced by the EDLC which is described in equation 3.1.

$$\Delta E = \frac{1}{2} C (V_i^2 - V_f^2) \tag{3.1}$$

In equation 1, ΔE is the EDLC's energy change in Joules, C is its capacitance in Farads, V_i is its initial voltage in Volts, and V_f is its final voltage again in Volts. The energy change is also the amount of energy needed to be returned to the EDLC during recharge to maintain its voltage the next pulsed loading. Rearranging the equation to calculate the voltage deviation, ΔV, of the bus yields equation 2:

$$\Delta V = V_i - \sqrt{V_i^2 - \frac{2\Delta E}{C}} \tag{3.2}$$

Where: $\Delta V = V_i - V_f$

Knowing the acceptable variation in the DC bus prior to operation allows the user to properly set the regulation controls for the battery and power supply currents.

Utilizing the power quality analysis metrics determined in the previously covered experiment for pulsed loads on isolated systems, the capability of the COTS HESM will be analyzed with respect to a pulsed load profile. The pulse load profile will have an active load discharge time of 5 s, followed by a 20 ms delay of inactivity. Prior to the start of the next

discharge state will be another 20 ms delay of inactivity. These 20 ms delays are to allow transition time for HESM state switching. The total inactive-load time is 1 second including the two 20 ms delay transition times. This profile was chosen as it is representative of the load profile of a typical 10 shot per minute pulsed load operation. The pulsed load specific energy storage will discharge into the pulsed load for up to one second and recharge for five seconds. The HESM load discharge state would be to recharge the specific pulsed load energy storage. Consequently, the HESM recharge time correlates to when the true or end use pulsed load itself is active. Since the experiments presented here focus on HESM, pulsed load will refer to the energy sourcing by the HESM directly. To evaluate the ability of the system to operate a pulsed load continuously, the individual pulse was repeated ten times in succession looking at the full 10 shots per minute and enabling the extrapolation of experimental data regarding bus voltages and line currents for operation beyond one minute.

Chapter 4

Experimental Results

4.1 Power Quality when Sourcing Pulsed Loads without a HESM

For testing the impact on power quality as a result of the pulsed power loads the experimental set with the two second 100% duty cycle load profile will receive the focus of the analysis with the other two 50% duty cycle sets compared to the two second base. To conserve space only the analysis of three experiments within each set will be shown. These are when the programmable load is set at the low 300 W setting, the high 2000 W setting and the final setting will be for 1300 W. This final setting was chosen based upon the base two second pulsed load profile experiments, where this was the programmable load value for which the current draw during the pulsed load remained the closest to constant.

The voltage and current waveforms recorded from the energy storage during each of the three programmable load settings are presented in Figures 4.1, 4.2, and 4.3 respectively. The DC load is pulsed to start just shy of the 1s mark represented by the green trigger signal in the figures. The charger is supplying current to the batteries prior to the pulsed discharge. This is indicated by a positive current value. When the IGBT's are closed, the charger supplies current to both the energy storage and the resistive load since the charger's pulsed output voltage is higher than that of the energy storage. When the charger output voltage is low, the energy storage is solely responsible for supplying current to the pulsed load. Current sourced out of the batteries is represented by a negative current value. The batteries state of charge (SOC) decreases slowly as the pulsed load active time increases.

During the experiment in which 300W is continuously drawn by the programmable load, the generator is able to supply power to the programmable load as well as charge the batteries and source the 2.3 kW pulsed load. As will be shown later, the quick transition from low power

draw to a high power draw induces high fluctuations in the generator output frequency. By the end of the two seconds, the current sourced to the pulsed load decreases from roughly 81 A down to 79 A due to the slightly decreasing DC bus voltage. Keep in mind that 300 W is roughly 10% of the generator's rated output power leaving the remaining 90% to source the pulsed load and batteries. As the batteries SOC, and therefore its terminal voltage, decreases the generator through the charger is able to source higher current values in order to try and maintain a constant voltage recharge. The increasing orange line drawn above the current waveform in Figure 4.1 is placed for presentation purposes only, to highlight the rate of increased recharge current sourced to the batteries.

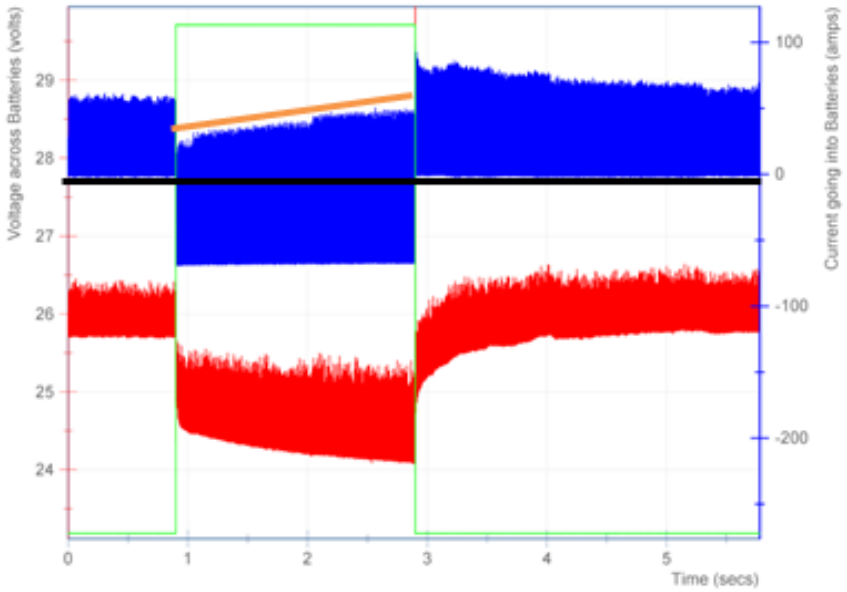

Figure 4.1 Energy Storage V&! for 300 W Load Experiment: Voltage (red) and Current (blue) during the 300 W AC programmable load test. Pulsed discharge time is highlighted by the green trigger pulse.

During the 1300 W experiment, it becomes harder for the generator to source all three loads, those being the batteries, the pulsed load, and the programmable load. When the charger output is high, it is able to source the programmable load and the pulsed load but its voltage sags at a similar rate to that of the batteries limiting its recharge current as the battery

voltage drops. The current supplied to the pulsed load by the charger decreases from 81 A down to 78 A in this experiment, as is highlighted again by the level orange line above the current waveform in Figure 4.2.

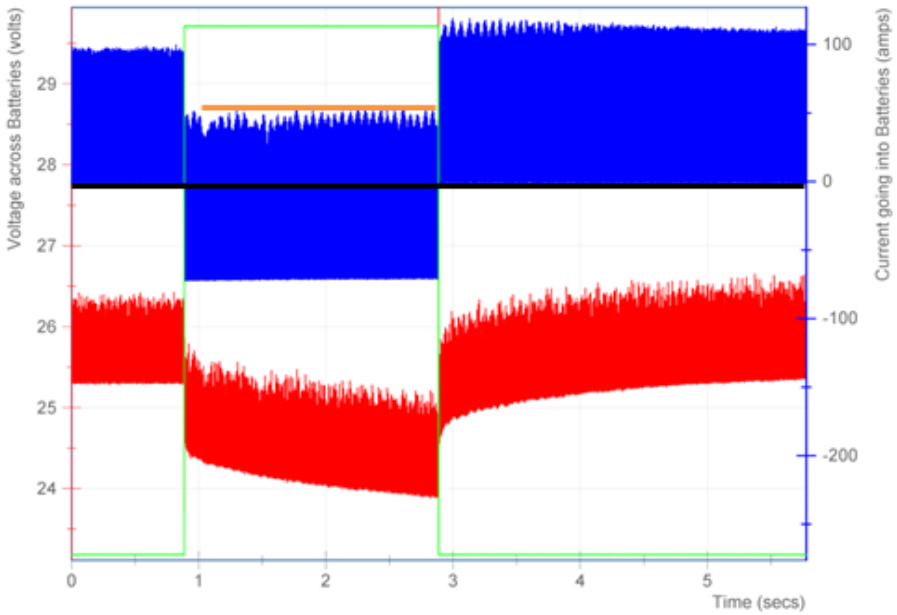

Figure 4.2 Energy Storage V&I for the 1300 W Load Experiment: Voltage (red) and Current (blue) during the 1300 W AC programmable load test.

Finally when 2000 W is sourced to the programmable load, the generator is unable to supply any recharge current to the batteries after providing power to the programmable and pulsed loads. The current supplied to the pulsed load by the charger decreases from 81 A down to 77 A. The generator output voltage sags considerably with the batteries actually regulating the DC bus voltage when the pulsed load is sourced. This is shown in Figure 4.3 where the orange line, the peaks of current supplied to the DC bus by the generator via the Outback power converter, actually decreases to zero quickly.

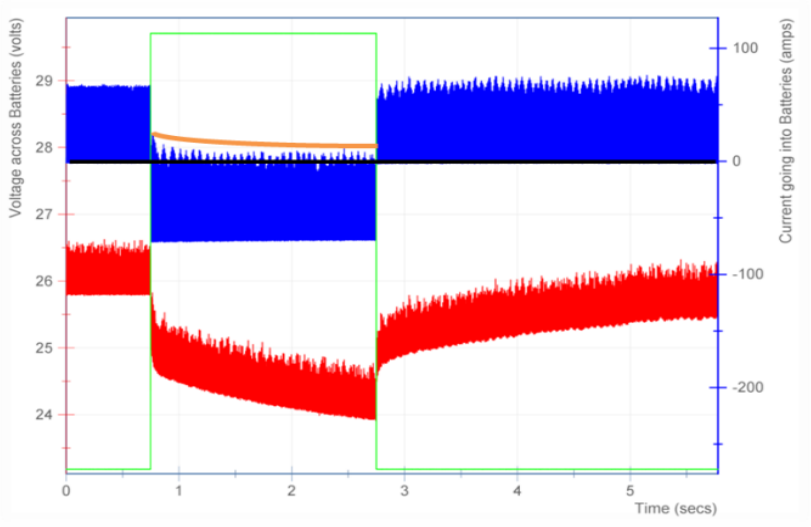

Figure 4.3 Energy Storage V&I for the 2000 W Load Experiment: Voltage(red) and Current (blue) during the 2000 W AC programmable load test.

As has been mentioned already, in all of the experiments the charger immediately increases its current output to the DC bus when the pulsed load is sourced. Plots of only the charger output current for the three tests above are shown in Figures 4.4 through 4.6 respectively.

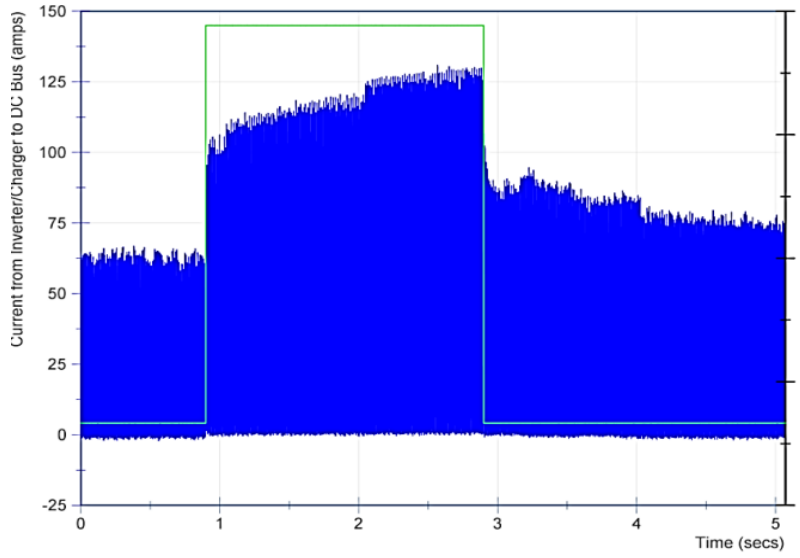

Figure 4.4 Charger Output Current during the 300 W Experiment.

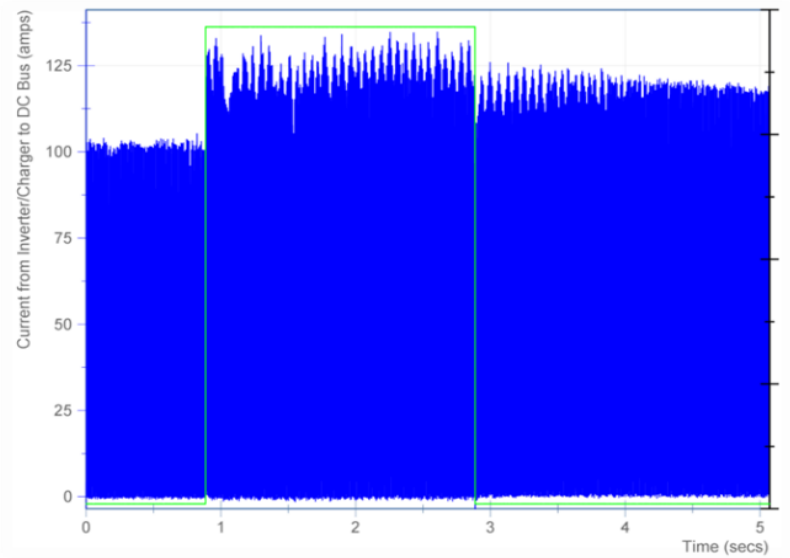

Figure 4.5 Charger Output Current during the 1300 W Experiment.

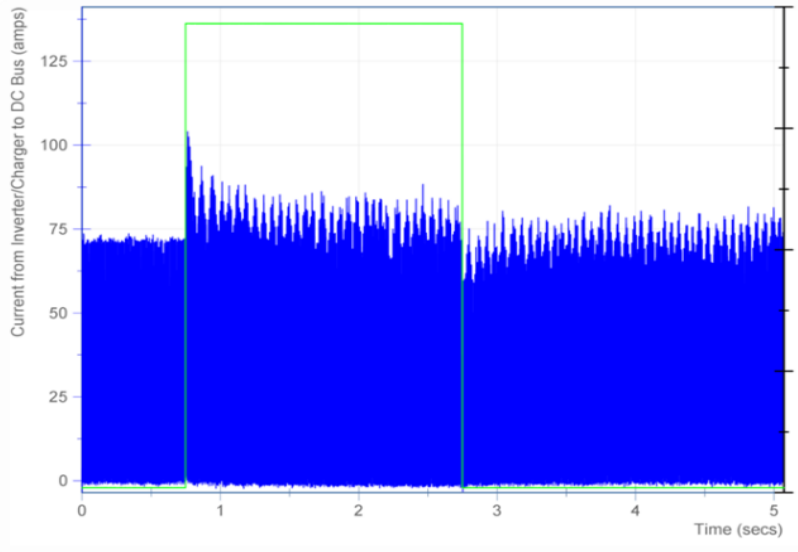

Figure 4.6 Charger Output Current during the 2000 W Experiment.

In the 300 W experiment, the charger current output increases throughout the sourcing of the pulsed load as the voltage on the DC bus declines. During the 1300 W test, the maximum charging current is quickly sourced and its peaks remain constant throughout the pulse despite the decrease in the DC bus voltage. When the 2000 W experiment is performed,

there is a quick spike in the output current followed by a very quick decline as the charger simply can't supply more power to the DC side of the system. This indicates that at the initial surge of current is more than likely supplied by the charger's output filter. Prior to the pulsed load, the power converter maintained a steady charge current however after the pulsed load terminates, the current is unable to quickly return to the previous steady charging current. Supplying the AC load is the power converter's first priority while any remaining energy, which is decreased with each subsequent experiment, is able to supply power to the DC bus. Ideally, this would mean that the generator supplies the AC load without power degradation and the DC bus will operate in a mostly independent fashion. But as it was established earlier this COTS power converter rectifies the AC input power onto the DC bus and then inverts what is on the DC bus into AC. Overall, this direct coupling of both AC buses to the DC bus through a single power conversion results in DC bus degradation having significant effect on AC bus status. The voltage recorded across the prog. AC load and generator, during the 300 W, 1300 W, and 2000 W experiments are presented in Figures 4.7 – 4.9 and Figures 4.10 – 4.12 respectively.

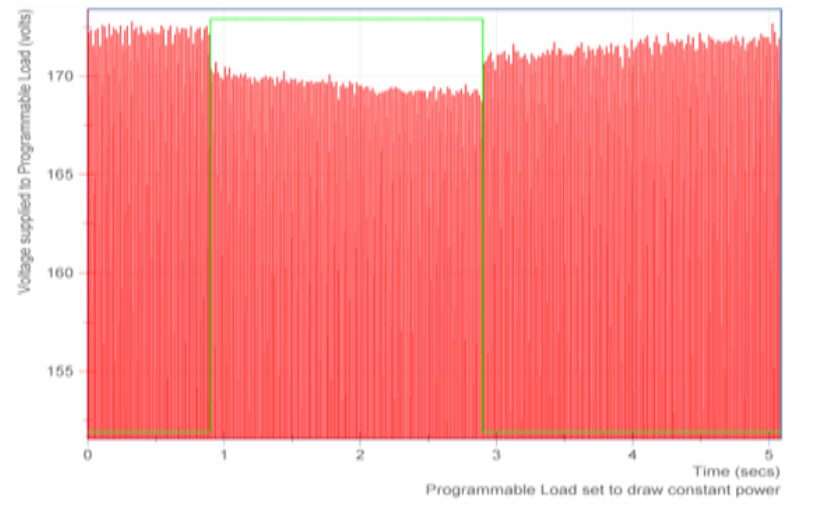

Figure 4.7 Programmable Load Voltage during 300 W Load Experiment.

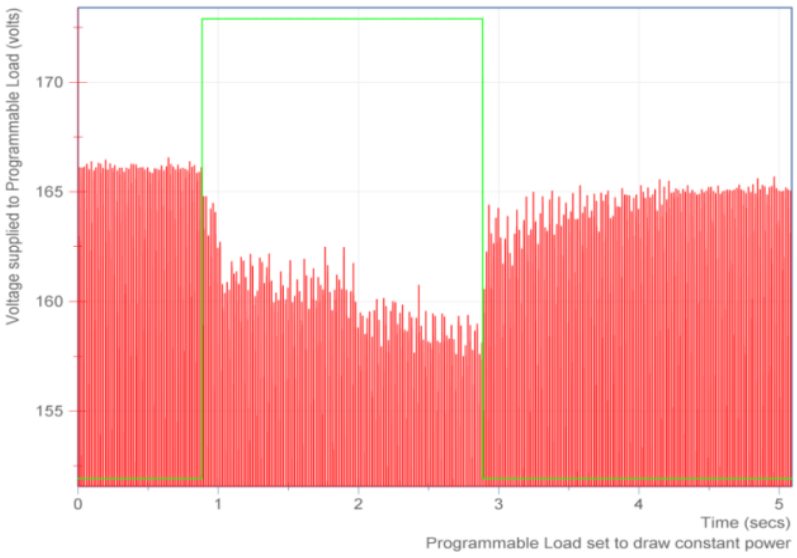

Figure 4.8 Programmable Load Voltage during 1300 W Load Experiment.

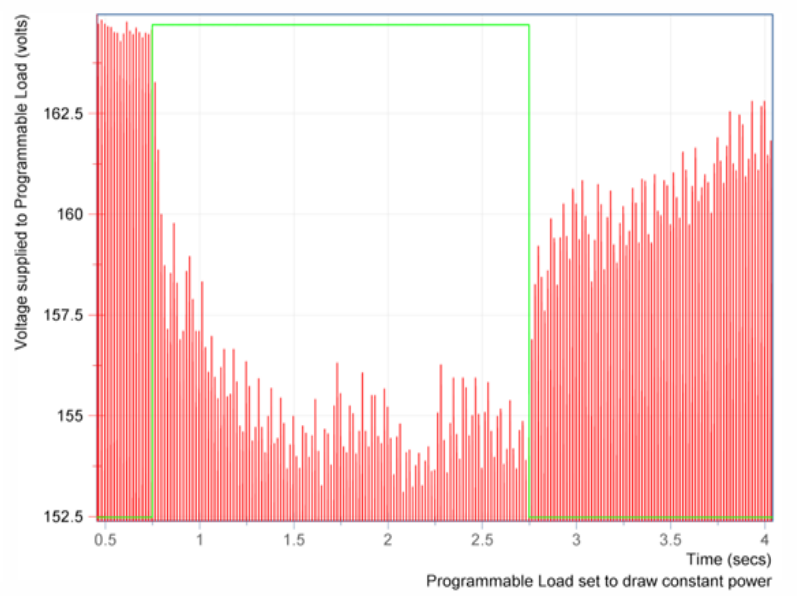

Figure 4.9 Programmable Load Voltage during 2000 W Load Experiment.

As expected, there are considerable sags in both of the AC voltages when the pulsed load is sourced. Sagging during and after the pulse occurs across all experiments and the severity increases as the AC load increases. Also, as expected, the current drawn by the

programmable load and sourced by the generator swells during the same time frame in order to maintain the constant AC power mode of operation. This is shown in Figures 4.13 – 4.15, respectively.

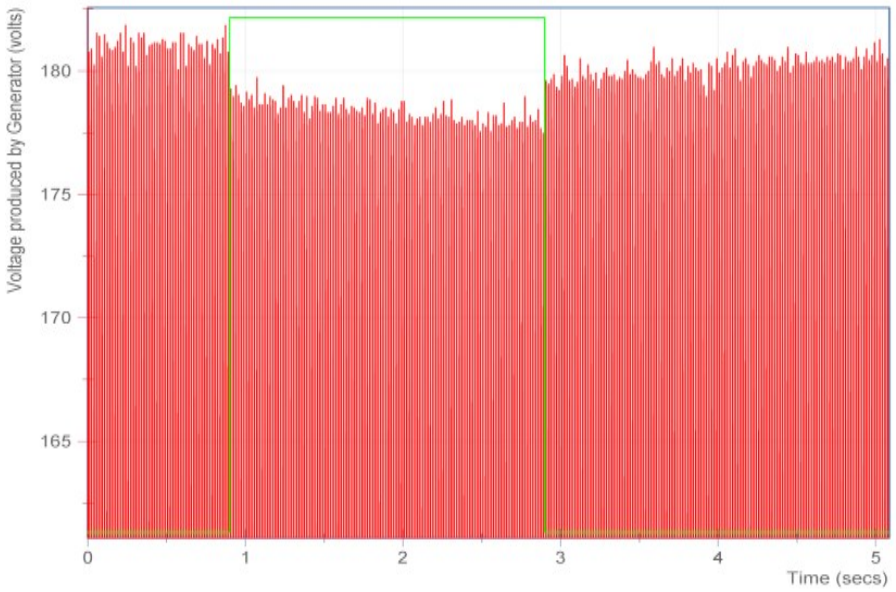

Figure 4.10 Generator Voltage during the 300 W Load Experiment.

Figure 4.11 Generator Voltage during the 1300 W Load Experiment.

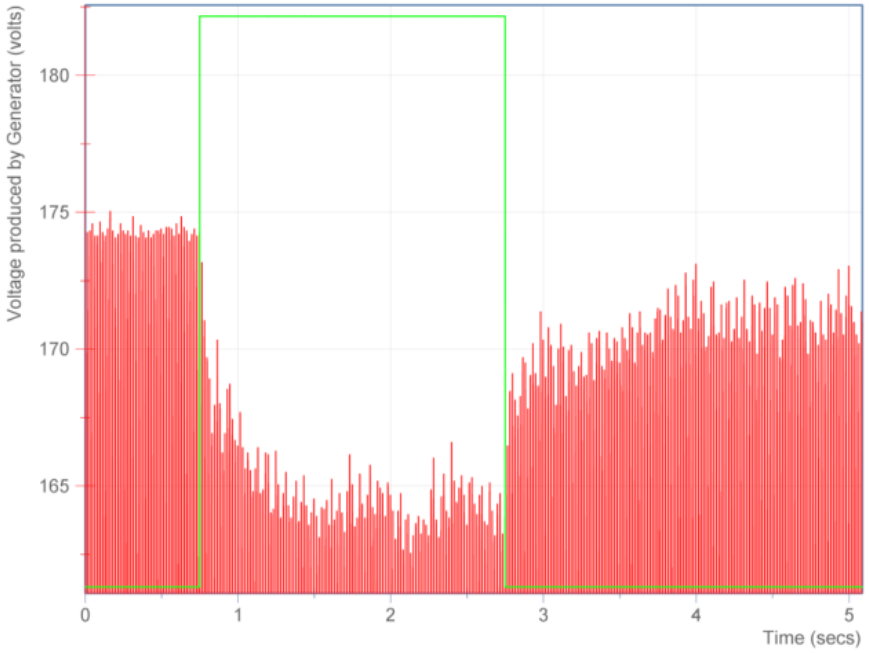

Figure 4.12 Generator Voltage during the 2000 W Load Experiment.

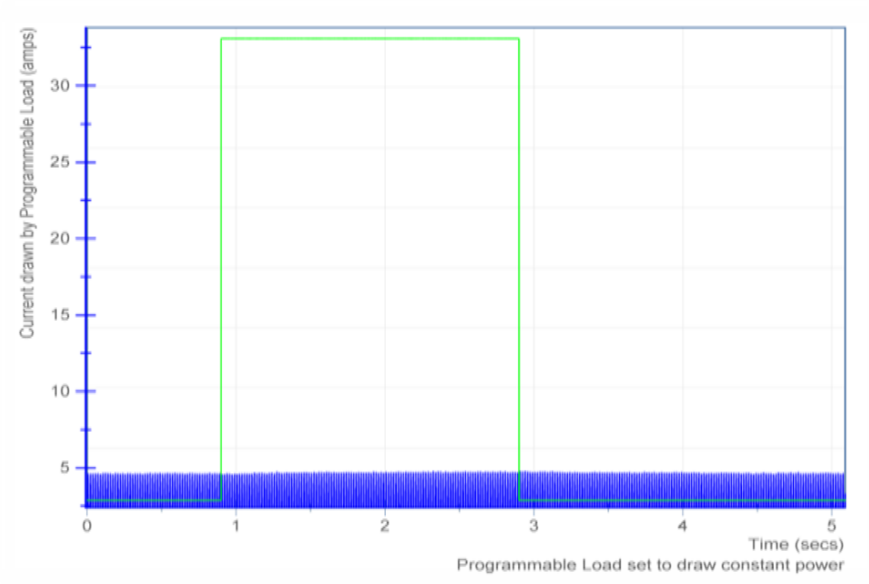

Figure 4.13 Programmable Load Current during the 300 W Experiment.

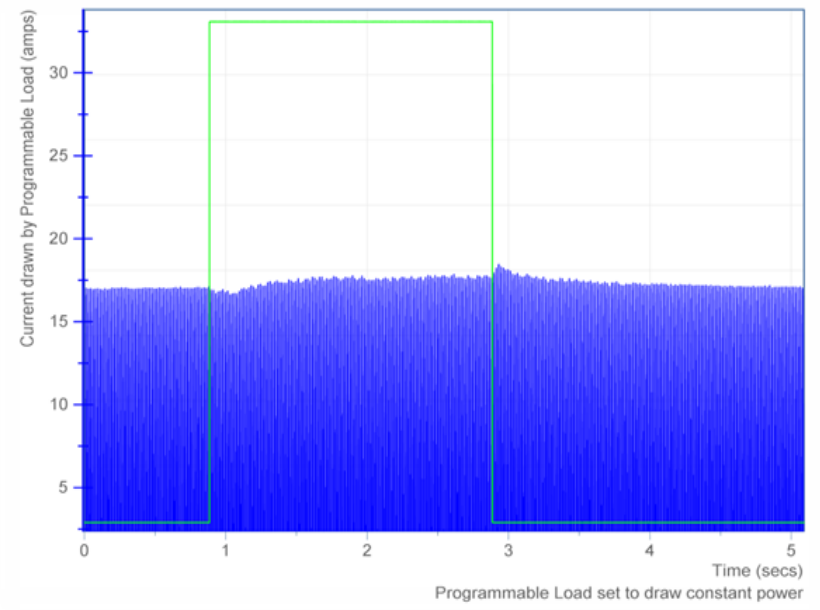

Figure 4.14 Programmable Load Current during the 1300 W Experiment.

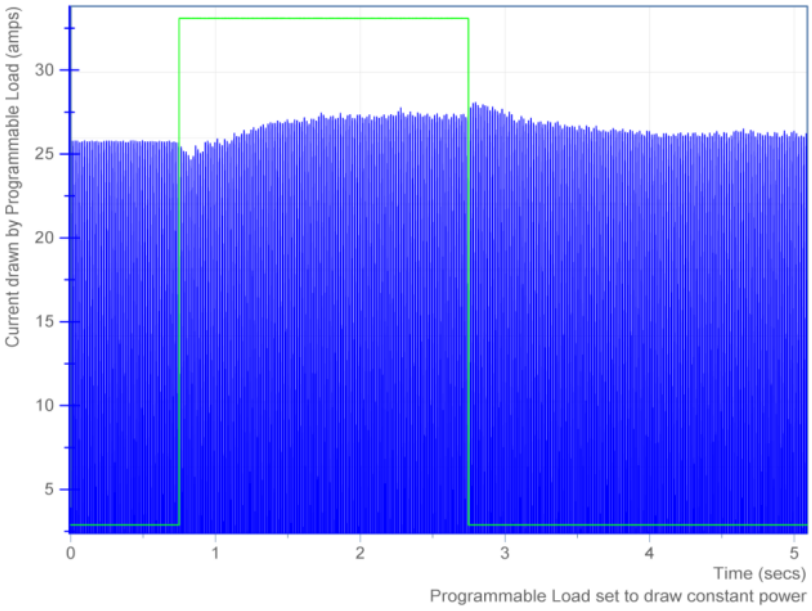

Figure 4.15 Programmable Load Current during the 2000 W Experiment.

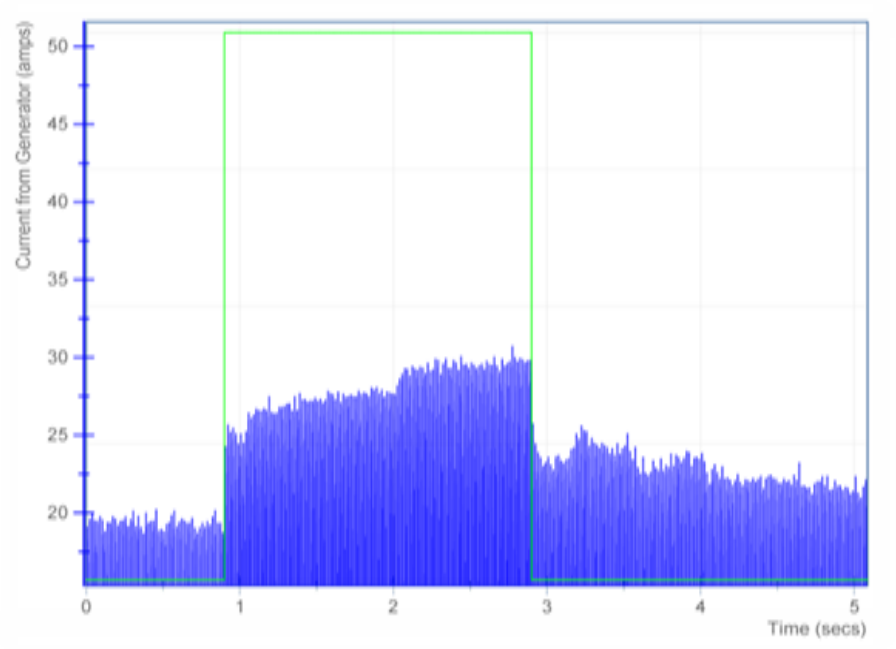

Figure 4.16 Generator Current during the 300 W Load Experiment.

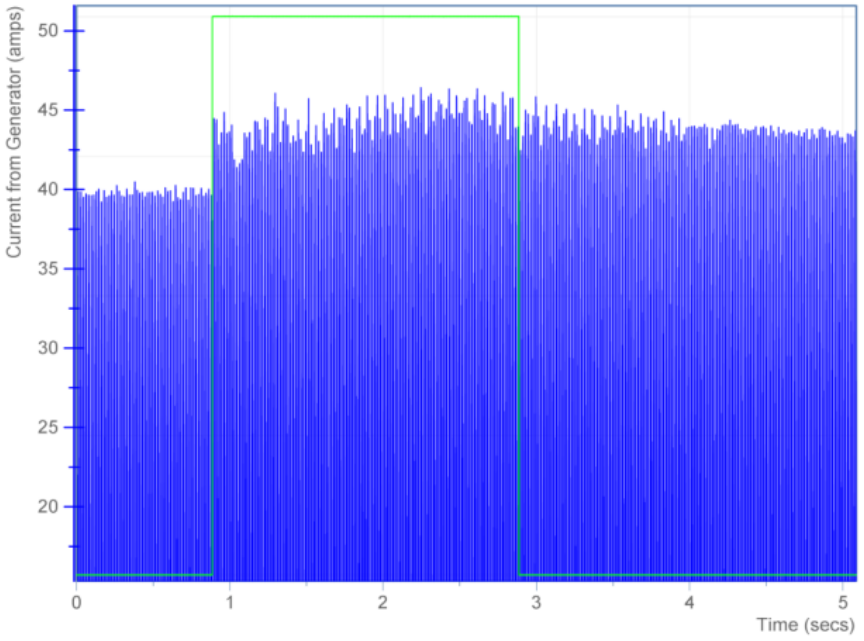

Figure 4.17 Generator Current during the 1300 W Load Experiment.

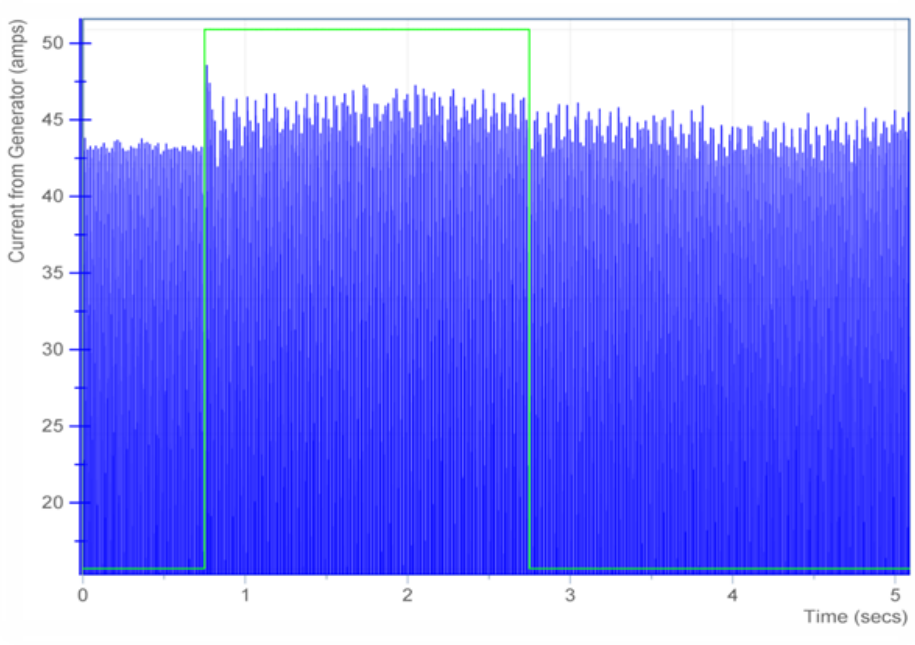

Figure 4.18 Generator Current during the 2000 W Load Experiment.

The current swells are most notable in the lower AC loading experiments. This is likely a result of the sudden transition from a low loading condition to a high loading condition when the pulsed load is triggered. The magnitude of the swell is limited of course by the maximum current the generator can source. When the 1300 W load is sourced, the generator still has some available power to source. During the 2000 W experiment, the generator starts at 64% its maximum power draw prior to the pulsed load, resulting in an even smaller amount of available power than in the 1300 W experiment. The pulsed load causes the current during and after the pulsed load to deviate much more compared to what it did before the pulsed load was sourced. Current deviation is not of consideration for most power quality analysis however, voltage deviation is and Figure 4.12 earlier is very reflective of generator voltage deviations.

In order to evaluate how the AC power quality is impacted due to these simultaneous loading conditions, the AC buses have been analyzed to see if they stay in accordance with the MIL-STD-1399-300B and IEEE-STD-519 specifications. The RMS values prior to the pulsed load and the minimum values recorded when the pulsed load is sourced are listed in Table 4.1.

Table 4.1 Generator and AC Load RMS Voltages for 2 s 100% Duty Load Profile

Voltage (RMS)	*300 W Exp.*	*1300 W Exp*	*2000 W Exp.*
Generator Max.	128.24 V	123.95 V	123.32 V
Generator Min.	125.65 V	118.19 V	115.42 V
AC Load Max.	121.90 V	117.43 V	116.30 V
AC Load Min.	119.50 V	111.53 V	109.21 V

The frequency tolerance listed in MIL-STD-1399-300B for a single phase, 120 VAC - 60 Hz power system is between 58.2 Hz and 61.8 Hz. The acceptable continuous voltage range is listed between 109 VAC and 121 VAC. For short durations up to 2 seconds, the allowable range is between 92 VAC and 138 VAC. In all of the experiments presented here, the AC bus voltages stayed well within the continuous bounds. During the 2000 W experiment, the continuous voltage range condition was nearly violated. The allowed AC voltage amplitude modulation is 2% and the allowable AC frequency modulation is 0.5%. The allowed total harmonic distortion (THD) is 5% and the ratio in percent of the greatest amplitude of a single harmonic over the fundamental frequency is 3% [46]. In comparison the standards listed in the IEEE-STD-519, which were developed for use in large scale electric power systems, have the same tolerances for the THD, highest single harmonic and frequency modulation, and a tighter tolerance of 0.5% on the voltage amplitude modulation [47,48]. Tables 4.2 and 4.3 present the results obtained from the frequency and modulation analysis of the two AC buses in the system. The analysis was performed using the techniques highlighted in the MIL-STD-1399-300B.

Table 4.2 Generator Power Quality Analysis for 2 s 100% Duty Load Profile

Generator	*300 W*	*1300*	*2000*
Amp. Modulation	1.11%	2.71%	3.68%
Freq. Modulation	0.60%	0.15%	0.24%
Highest Harmonic	0.70%	0.67%	0.59%
THD	1.08%	1.24%	0.89%

Table 4.3 Programmable AC Load Power Quality Analysis for 2 s 100% Duty Load Profile

AC Load (Voltage)	*300 W*	*1300*	*2000*
Amp. Modulation	1.21%	2.74%	3.72%
Freq. Modulation	0.85%	0.75%	0.78%
Highest Harmonic	0.76%	0.44%	0.52%
THD	1.02%	0.66%	1.02%

The generator's open circuit fundamental frequency is 59.9 Hz. The THD and the value of the highest harmonic, the third harmonic, all fall within the bounds set by the MIL-STD-1399, but are out of the bounds set by IEEE-STD-519. The voltage amplitude and frequency modulation values fall out of bounds for the AC load in nearly all of the experiments performed, however the generator is only out of frequency specification during the light load experiment and out of voltage specification during the higher load experiments. The differences in power quality values between the AC buses also show that the inverters pass thru is not a direct connection between its AC input and output buses. The generator shows increased frequency stability with increased loading and as expected the voltage modulation falls as the load increases. None of the RMS voltages measured fell out of the specified voltage range given in Figure 4.11 within the MIL-STD-1399-300B [46]. The generator's best power quality was observed when the initial loading was high. The quality of the power received by the AC load was best when medium power levels were sourced. The power quality results of the 50% duty cycle pulsed load profiles for both 30 ms and 400 ms periods follow the same overall pattern and are given in the following tables.

Table 4.4 Generator Power Quality Analysis for 30 ms 50% Duty Load Profile: Violations in red

Generator	*300 W*	*1300*	*2000*
Amp. Modulation	1.36%	3.17%	1.84%
Freq. Modulation	0.63%	0.24%	0.24%
Highest Harmonic	0.69%	0.72%	0.59%
THD	1.20%	1.12%	0.88%

Table 4.5 Programmable AC Load Power Quality Analysis for 30 ms 50% Duty Load Profile

AC Load (Voltage)	*300 W*	*1300*	*2000*
Amp. Modulation	1.38%	3.29%	1.84%
Freq. Modulation	0.76%	0.75%	1.02%
Highest Harmonic	0.73%	0.42%	0.52%
THD	1.09%	0.67%	1.02%

Table 4.6 Generator Power Quality Analysis for 400 ms 50% Duty Load Profile

Generator	*300 W*	*1300*	*2000*
Amp. Modulation	1.11%	5.33%	3.05%
Freq. Modulation	0.60%	0.24%	0.27%
Highest Harmonic	0.66%	0.68%	0.55%
THD	1.40%	1.14%	0.87%

Table 4.7 Programmable AC Load Power Quality Analysis for 400 ms 50% Duty Load Profile

AC Load (Voltage)	*300 W*	*1300*	*2000*
Amp. Modulation	1.21%	5.21%	3.17%
Freq. Modulation	0.85%	0.93%	0.66%
Highest Harmonic	0.67%	0.48%	0.57%
THD	1.07%	0.66%	1.08%

The power quality in the pulse train load profiles has greater power quality deviation at the low and intermediate loading level but superior power quality performance at the high loading level. When the loading is light, the transients caused by the pulsed profile produce a noticeable negative impact on the system. As the pulsed load becomes less of the total load demand the intermediate times of the inactive pulsed load allow for a brief window of partial system recovery. Comparing the two pulsed profiles power quality improved as the duration between inactive load states decreased.

Unless the COTS AC/DC converter used has true AC pass thru, AC load power quality is independent of generator power quality. AC pass thru is the connection of the AC output of the power converter to the input so that the AC source directly supplies the AC load. To augment this output power with energy storage the AC output power of the internal inverter

must match output phase, frequency, and voltage to the generator input. In checking for true AC pass thru, start by looking at what will the easiest of the three parameters to measure. Looking back at Table 4.1 the AC load bus in all cases had a lower voltage than the generator bus. The AC load bus was closer to the nominal 120 VAC and the generator bus ran higher. This further indicates that the COTS power converter does not directly pass thru AC input power to the output. The indirect AC pass-thru is an efficient use of internal power electronics under normal load conditions. The AC input is rectified onto the DC bus and energy storage and then inverted back into AC power. By having the DC energy storage as the center of the system, the energy storage can respond quickly to changes on either AC bus more quickly and provides a guaranteed stable source of power to support the power electronics and controlling computers.

This conclusion is further supported by the COTS cessation of operation as soon as the DC energy storage was disconnected even when supplied with AC power. The result is that the AC load power quality is directly dependent upon the energy storage and if it remains within the acceptable voltage range of the inverter. The decrease in generator side power quality is a result of both delays in state transition of the COTS power converter as well as nature of the experiment which increased the AC loading level for the observation of power quality under stressed conditions. In a fielded application, the system energy storage and generation would be sized for the load and any COTS power converters used with pulsed power systems should not have long delays before state transition as is more desired in residential use. The overall result is that when the energy storage is implemented as a core component the AC power quality becomes dependent upon sufficient available energy. For energy storage devices such as batteries and capacitors, the energy stored within for a particular model is reflected in the device voltage. Power quality and the long term feasibility of continued system operation can be determined by the current DC voltage and the rate of decay.

4.2 Evaluation of the COTS HESM with Pulsed Loads on Power Quality

As mentioned earlier the evaluation of the COTS HESM will be done utilizing a known pulsed load profile. The pulsed load profile has a one second active state and five second recharge state which translates to the electrical grid, including the HESM, as five seconds to supply energy to the pulsed load's energy storage. The one second active time for the load provides a small window during which the HESM can be recharged. Additionally, all switching of the power converters must be performed during the time when the pulsed load system is isolated. The data collected will be subsequently presented and analyzed.

The following graphs consist of data recorded during the experiment. Figure 4.18 shows the rise and fall of both the DC load bus voltage with the capacitor and the battery bus voltage across the entire pulsed load profile. The batteries have almost a 5.5% voltage drop when loaded while the EDLC has roughly a 3% voltage drop between the active and inactive load states. The overall voltage drop of the EDLC during the HESM experimental operation has the form of an exponential decay. This is due to both the decay constant of a capacitor and the fact that the EDLC was not fully recharged between each pulse. In order to recharge the capacitor fully, roughly five times the average current taken out of it during the 5 s discharge must be applied back into it during the 1 s recharge profile.

The capacitor's exponential voltage drop is reflected on the load bus voltage in Figure 4.19. At the beginning of the process, the change in voltage is more significant than it is as the process unfolds due to the decreasing voltage. The small oscillations induced on the voltage traces are a result of the 31.25 kHz switching frequency of the DC/DC converters.

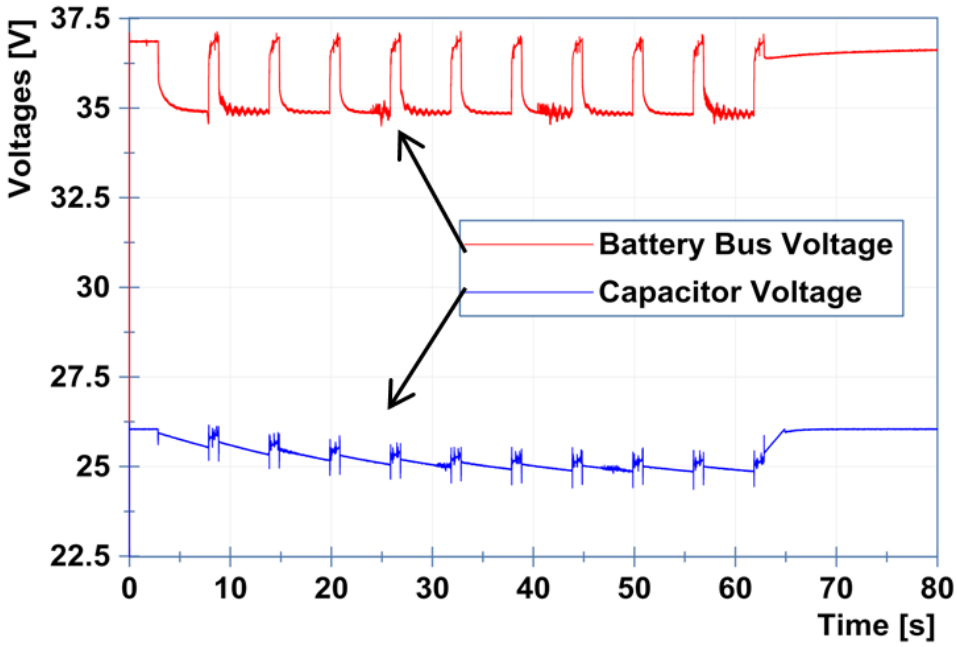

Figure 4.19 HESM Bus Voltages: Battery and load voltage profiles during ten consecutive 5 s active, 1 s inactive pulsed load states.

Figure 4.20 displays plots of the system currents recorded during the ten experimental cycles. While it may initially appear that the nodal currents do not sum up to the pulsed load current, it should be noted that the battery current plotted is that measured into the buck DC/DC converter. This current was selected as it represents the current drawn from the batteries which is of higher importance than the current supplied out of the DC/DC converter. It is also worth noting that the power supply current remains constant. Even during the periods of inactivity, the capacitor is directly connected to the power supply thereby sinking current from it even when the load and recharge converters are disabled. Once the recharge converters are enabled, the current into the capacitor decreases as current is diverted into the batteries. The constant output of the DC power supply reflects the steady state current received by the HESM under the assumption that exterior loads are constant during the pulsed load operation. If exterior loads are not constant the both the current limitations on all the COTS buck converters within the HESM would dynamically adjust to maintain as close as possible the direct output of the

generator to its nominal. For constant exterior loads, the generator continues sourcing power at its peak efficiency while recharging the energy storage devices.

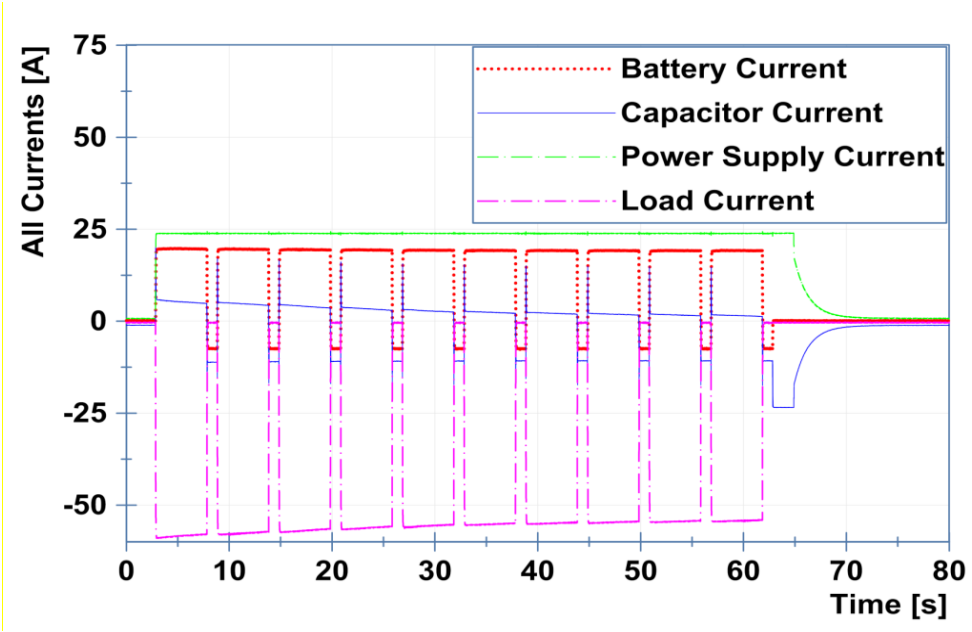

Figure 4.20 HESM System Currents: Sources and load current profiles during ten consecutive pulsed load states.

An interesting occurrence taking place in this circuit is the flow of current taking preference towards the battery over the EDLC despite the low impedance of the EDLC. Initially, it was thought that the high specific power of the EDLC and relatively lower ESR than the batteries would enable it to absorb high currents while limiting that supplied to the batteries to rates within their rated recharge values. In early experimentation this was found to not be the result. As highlighted by the right circle in Figure 4.21, while the discharge currents follow what was expected the recharge currents do not.

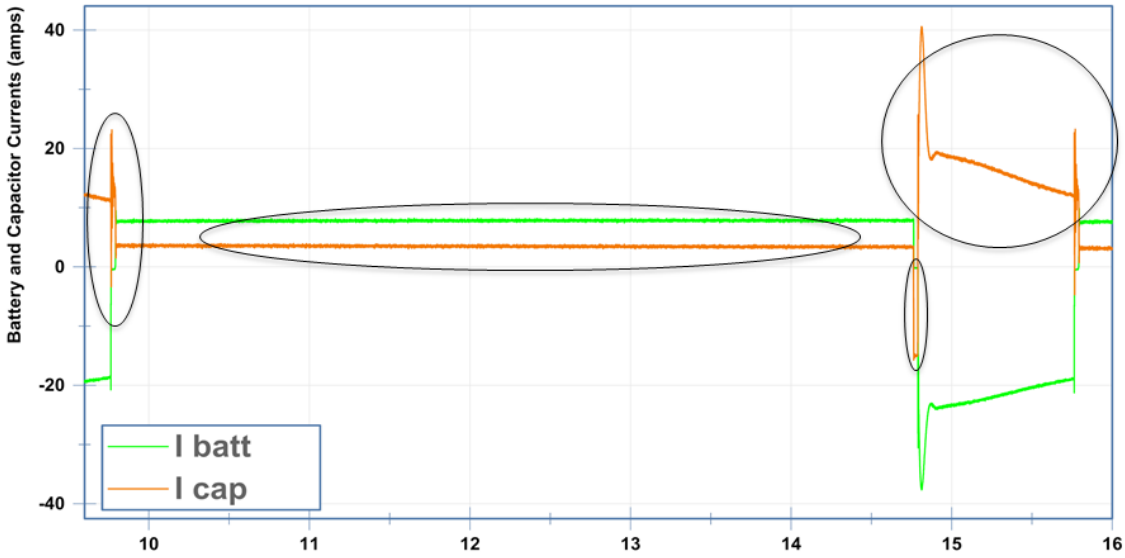

Figure 4.21 HESM Energy Storage Unregulated Currents: Battery and Capacitor currents in a single pulse of the pulsed profile without recharge current limitation

Initially during recharge the capacitor absorbs the sudden transient change in current direction, as desired. However, the reason is not due to power or energy densities but rather that the recharge path for the batteries have a switch delay before turning on. The converters respond within microseconds of receiving an enable/disable signal. Their subsequent internal transition time to respond to full power flow takes 5 ms. Once the battery recharge path via the boost converter is connected the capacitor ceases to be recharged and in fact supplies current to charge the batteries at higher rate than even the pulsed load demanded. This is because an ideal DC/DC converter has zero input impedance and infinite output impedance. Although this converter is not ideal, it has input impedance closer to zero than even that of the EDLC's ESR. This was considered a possibility but due to propriety control of the internal workings of the COTS converters was not a definitive occurrence. The result is a positive observation as this improves level of control and is heavily desired. The current of the unregulated capacitor can be controlled by controlling the more dominant current paths.

Due to the lower input impedence of the converter compared to the impedence of the capacitor there are impacts on system stability for unregulated recharge currents. Which can be seen in Figure 4.22 where the output bus, capacitor, voltage drops considerably as the test progresses without any stabilization or leveling as could be seen in the same experiment with the addition of a recharge buck converter for current limiting in Figure 4.20.

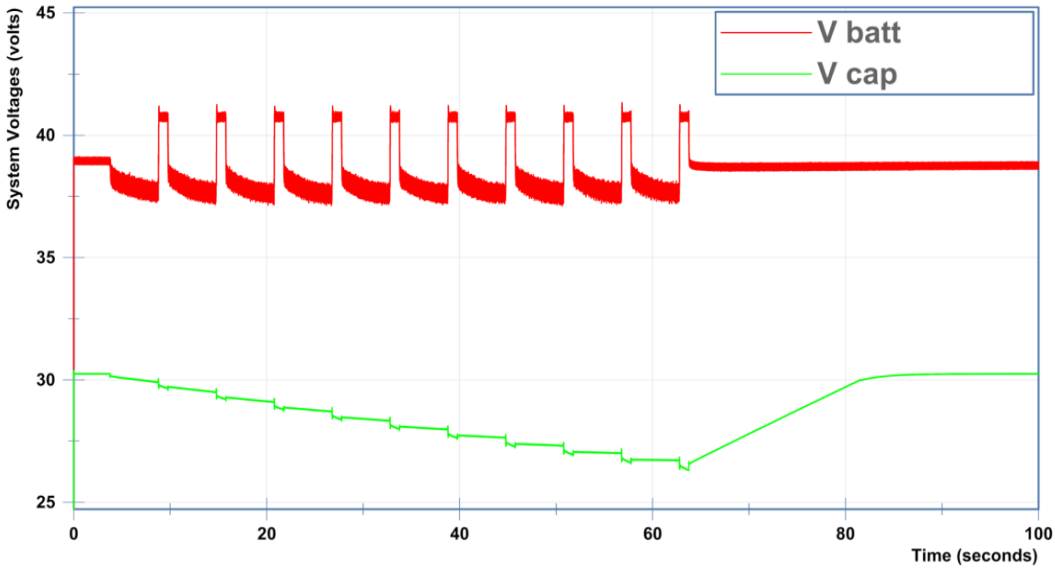

Figure 4.22 HESM Unregulated Bus Voltages: Battery and Capacitor voltages across pulsed load profile without recharge current limitation

In the experiment without the recharge buck converter it was observed that in an active HESM a small fraction of time is required to charge internal control devices and filters when enabled and this delay should be accounted for in the pulsed power system deployment when not in an energized initial condition. Looking at the first pulsed loading in Figure 4.23 it can be seen that the HESM was not initially loading the primary power generation at the desired level reflecting optimal loading.

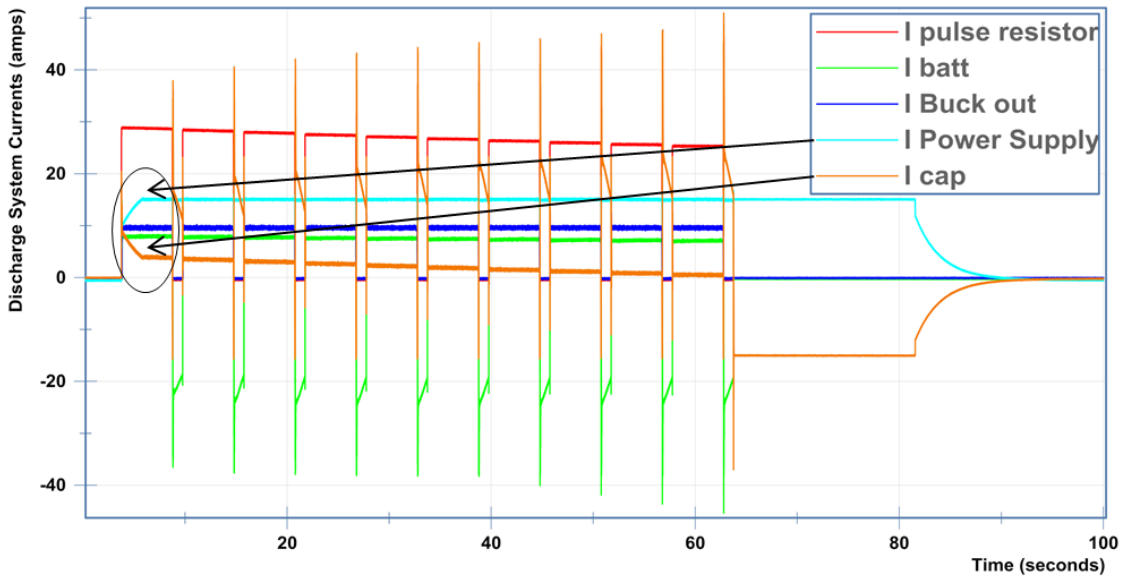

Figure 4.23 HESM System Currents for Unregulated Recharge: Overall decay trend for 5 sec. discharge currents for experiment without recharge current limits and charged initial conditions

Charging of the energy storage components within the converters is initially performed by the capacitor which decreases the HESM output voltage. The power supply was connected and full current draw allowed prior to the start of the pulsed load profile. A fully charged HESM is unable to act as a load for excess power from the primary power generation. Thusly, in the experimental setup presented here the power supply was idle. In the initial pulses the capacitor current mirrors the power supply with respect to the buck converter output current. In which the HESM by design automatically uses the capacitor to cover for deficiency in primary power to supply the pulsed load. For the experiment with recharge current limitation implemented the experiment was run with the HESM energy storage not in a fully charged state.

A zoomed in view of the currents during a single 5 s discharge is shown in Figure 4.24. It can be seen that at the start of the pulsed loading, there is a spike in the current sourced by the EDLC whereas the batteries have a quick but gentle rise up to their full current sourcing level. This is exactly the desired result from this configuration. The high power density of the

EDLC coupled with the converter current limiting enable it to respond in this manner to a pulsed load and take advantage of the capacitor's ability to source high transient currents without impact on life-cycle. In the HESM, this is achieved by the capacitor covering the initial transient and peak-shaving the current of the primary energy storage thereby relieving the stress generated on the battery's internal chemistry by both pulsed discharges and more importantly transients during recharge. Thus, the COTS HESM demonstrates the requirements regarding battery current control to prolong the battery's cycle life considerably.

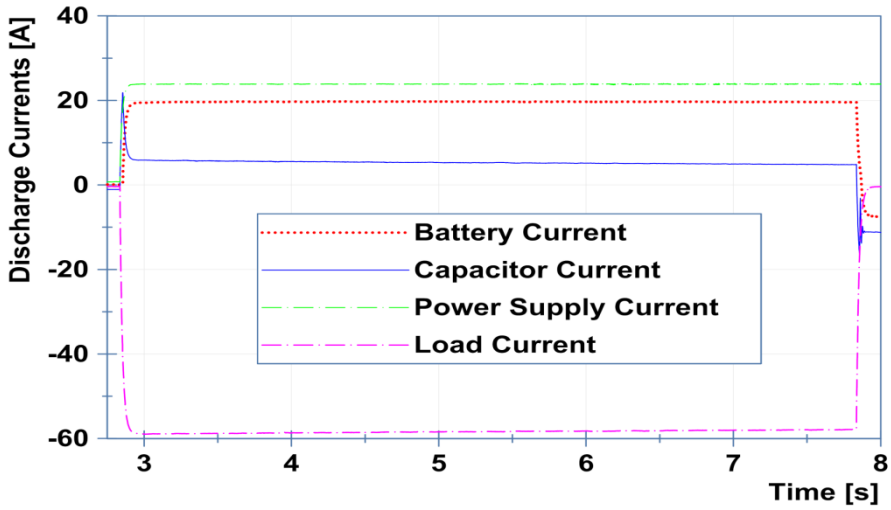

Figure 4.24 HESM Discharge Currents: Waveforms during a 5 s pulsed load active state. Of note is the time just before the 3 sec mark showing the peak of the EDLC's output at the start of the current sourcing.

Unfortunately, the straight forward but indirect current control of the unregulated EDLC current does not also apply for voltage control of the output bus. Rather the capacitor voltage is controlled by the total amount of charge in the energy storage device as given by equation 4.1. Resulting in COTS HESM having the capabiliy to control the amount of charge placed into the EDLC but as it cannot control the loads, the charge removed is observable but not controllable.

$$V = \frac{1}{C}\int_{t_0}^{T} \frac{dQ(t)}{dt}\,dt + V_i \qquad (4.1)$$

Where: V is the current voltage on the EDLC, V_i is the initial EDLC voltage, C is the capacitance of the EDLC, and Q(t) is the amount of charge present on the plates of the EDLC at a given time. The bus voltage for the EDLC is set solely by the voltage of the power supply, which like the AC to DC Outback power converter will act as a non-stiff source when the current limit is reached by allowing the output voltage to sag. As energy is sourced by the HESM both battery bank and EDLC voltages decrease during any individual time the pulsed load is active, shown in Figure 4.25. The simplified equation describing this discharging capacitor voltage is:

$$V = V_i e^{-\frac{t}{rC}} \qquad (4.2)$$

Where: t is the amount of time that has passed and r is the ESR of the EDLC.

This change is an exponential decay, but cannot be seen by looking at a single individual pulse and in the data appears as a small linear decrease in voltage. With the bus voltage being supported by both converters and the power supply the change in EDLC voltage per pulse is small and thus so is the withdrawal of energy with respect to the rated capacity of the EDLC. Looking back at Figure 4.19 and across all of the pulsed load states an exponential decay curve can be seen.

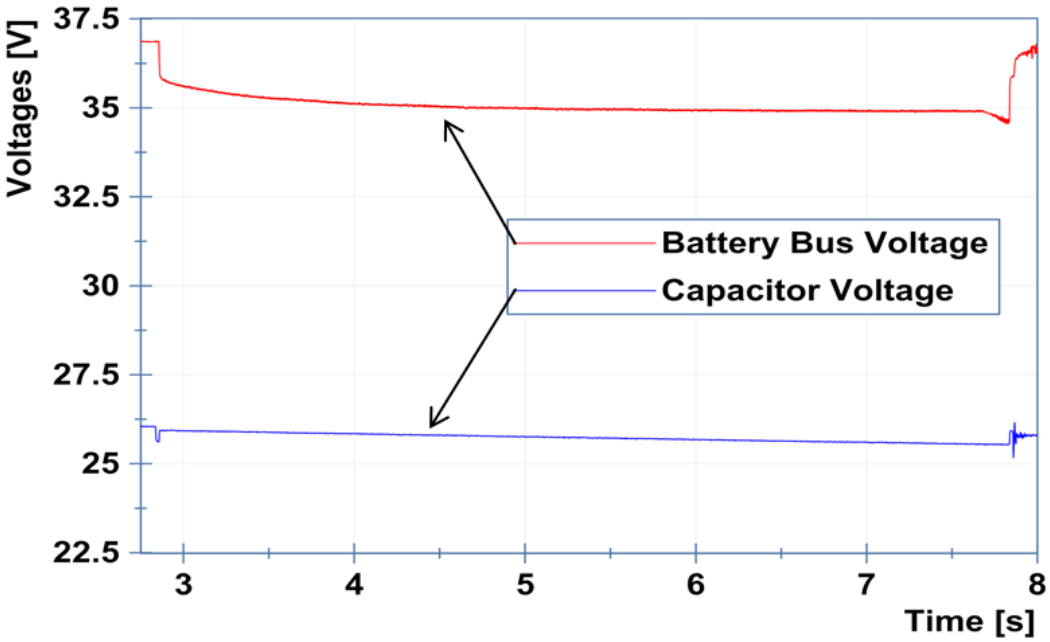

Figure 4.25 HESM Discharge Voltages: Battery bank and electric double layer capacitor voltage decrease during the active load state.

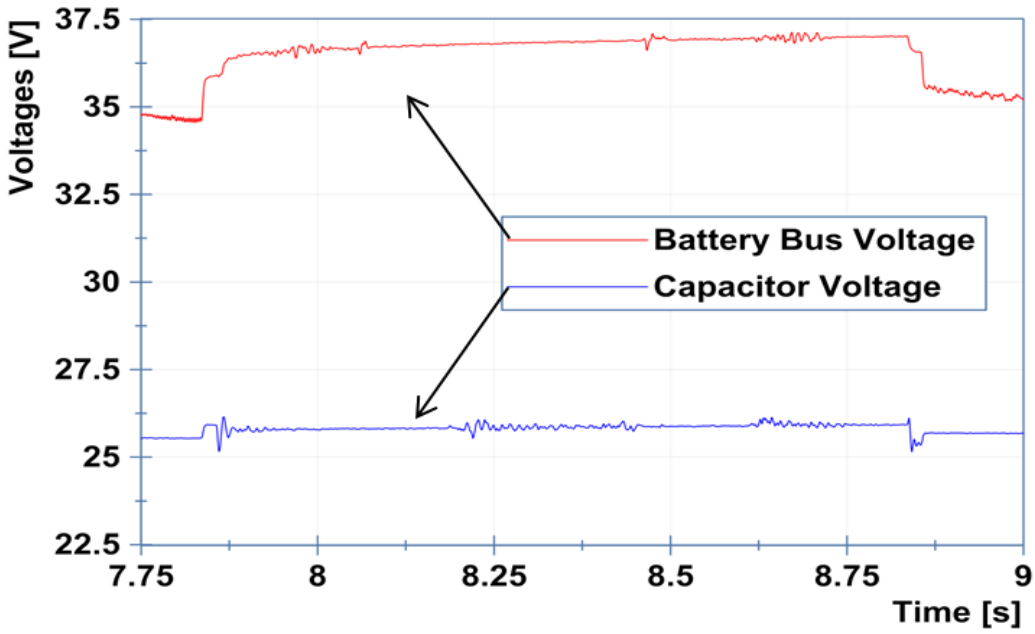

Figure 4.26 HESM Recharge Voltages: Battery bank and EDLC voltage rise during pulsed load inactive state.

During the inactive load state the recharge voltage of the battery bank increases significantly more than the recharge voltage of the EDLC as shown in Figure 4.26. By design, the power supply was chosen to operate at a constant voltage and current to replicate the maximum operation of the primary power with constant loading exterior to the HESM and pulsed load. The larger the increase in battery bank voltage between nominal and the recharge voltage the greater the amount of charge restored per pulsed load cycle. This was possible as a result of the battery bank being a regulated source via the recharge converters. As mentioned earlier, the unregulated EDLC is capable of faster response times, but as shown the lack of regulation limits the system capability to force a recharge of energy into the EDLC during the load inactive state that compensates for charge drained.

The currents measured during a single 1 s recharge pulse that occurs during the inactive-load operation are shown in Figure 4.27. Although there is no direct regulation of current flow into the EDLC during the inactive-load operation, by controlling the current into the batteries, the excess current sourced by the power supply is forced into the EDLC, thereby replenishing its charge.

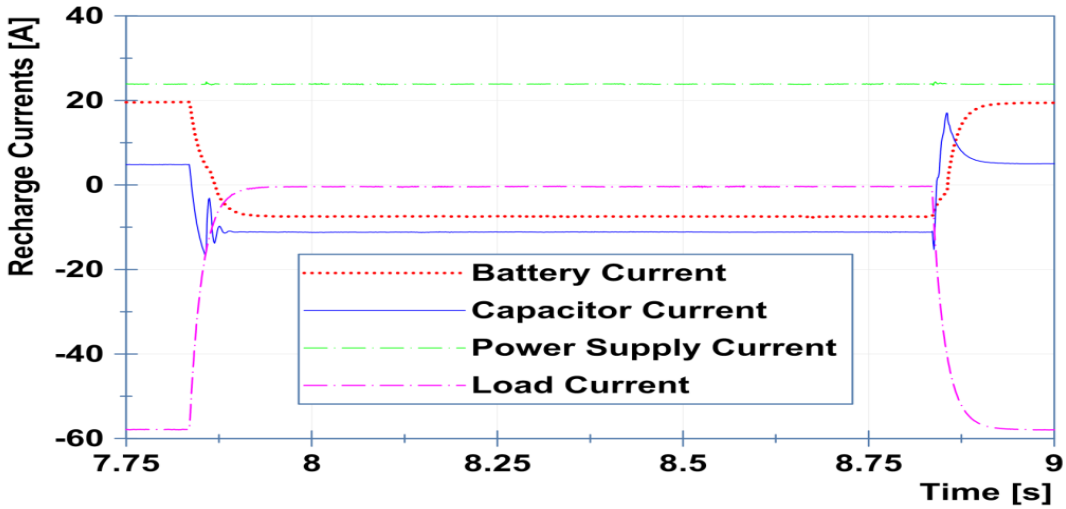

Figure 4.27 HESM System Currents with Recharge Regulation: Shown during pulsed load inactive state.

Initially, there is an overshoot in the current sourced to the EDLC. The current is a combination of the full 25 A available from the power supply and the current out of the battery bank discharge buck converter until it is disconnected minus the residual fading pulsed load current demand. As it was in the currents, it can be seen that the EDLC handles all the transient energy storage demands, as can be seen in Figure 4.28.

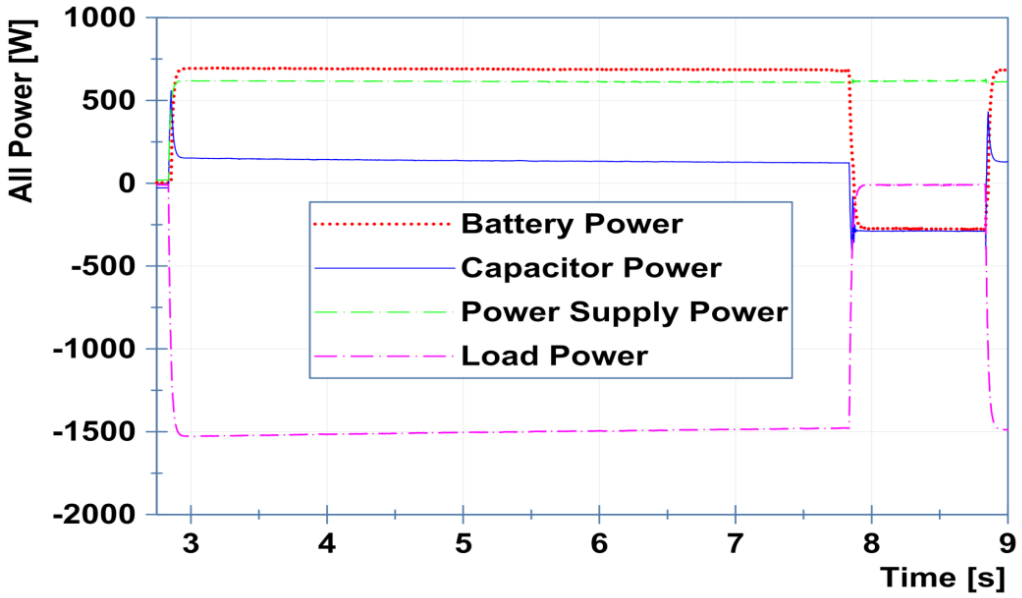

Figure 4.28 HESM Single Pulse Power Flow: Through sources and loads during a pulse.

With near constant DC bus voltages during either the active or inactive load states, the currents also correlates to the power flows. The power flows enable easier internal comparative system analysis by utilizing conservation of energy. There are losses not shown in Fig. 9 due to the power converters, but the COTS employed have power conversion efficiencies in the mid to upper 90 percentile. During the inactive loading, the power into the battery bank and capacitor are close to the same value.

Chapter 5

Summary & Conclusions

A HESM was constructed to test the impact on power quality on an electrical grid with hybrid energy storage when pulsed loads are operated. A baseline test was established using COTS components to construct a MicroGrid of comparable size to observe the impact of pulsed power loads and obtain a baseline analysis of the power quality without a HESM. The results showed a negligible impact on harmonics but violations of power quality standards for voltage and frequency deviations. These deviations increased with loading on the AC side and decreased with loading on the AC generation side as the generator was operated closer to its rated value. This illustrates one reason behind the desire to employ a HESM: so that primary power generation can be operated at its most efficient rated output. Following this, a HESM was constructed using COTS components to complete the analysis.

The results of the HESM pulsed load experiments show that with the basic power converter controls of enable/disable, voltage gain and current limit, the output voltage can be held within the operational range of DC/AC power inverters and thus preserve output power quality. Building off the work of Gao et. al. [11,19], a time average current scheme was used to calculate the recharge current limits based upon the discharge profile and subsequently based upon the size of the COTS components used, what would be an optimized nominal power draw for the MicroGrid with HESM based upon the pulsed load profile. In a laboratory setting, the time average scheme adjusted the system input based upon system sizing, in field implementation the scheme would be applied the other way.

When implementing two or more energy storage technologies, their individual limitations are overcome. The EDLC successfully covered all transient currents and absorbed recharge current in excess of the desired recharge rate of the batteries. Looking at the work of Biju et. al. [24] by limiting the exposure of the batteries to high transient currents and in

particular recharge currents, they retain more of their nominal cycle life than they would as the sole energy storage device.

Moving forward, it would be interesting to examine the performance gains in both overall capabilities and power quality stability when implementing the latest in energy storage device technologies such as lithium-ion batteries instead of lead-acid and lithium-ion capacitors instead of EDLCs. Additional experimentation can further implement the MicroGrid concept and expand the repertoire of the HESM by employing and controlling the management of renewable energy sources such photo-voltaics, wind turbines, and fuel cells. Fuel cells have been in discussion amongst HESM research in various topologies and experiments employing the control of three or more energy storage devices within a HESM could provide valuable development of control principles and standards for future HESM implementations. To stabilize the HESM bus voltage and bypass charge rate limitation on the capacitor due to time constants, power converters can be placed between the capacitor and the PoCC. The last major aspect for future experimentation would utilize more complex load profiles. The repeated profile could be repeated several times in a grouping and various durations between groups implemented. This would allow for extended duration stability analysis and allow lower recharge current into the battery to be viable since there will be significant off times between pulsed load usages for recharge. Such profiles could include delayed primary power support where the HESM is responsible for completely supplying the pulsed load for a short duration. The pulsed load profile can be expanded to include inrush currents of system motors in addition to the constant profile. Custom load profiles can also be implemented on both the DC and AC buses. The area of HESM research still has a ways to go and research employing COTS devices can expedite the process.

References

[1] J. Thongam, et al. "All-electric ships—A review of the present state of the art," *Ecological Vehicles and Renewable Energies (EVER), 2013 8th International Conference and Exhibition on* , vol., no., pp.1,8, 27-30 March 2013

[2] US Destroyers Get a HED: More Power to THEM!, *Defense Industry Daily*, [online] 09 May 2012, http://www.defenseindustrydaily.com/US-Destroyers-Get-a-HED-More-Power-to-Them-07142/

[3] E. Lundquist, “DDG 1000’s Integrated Power System Software, Hardware come Together in Successful Test,” (Aarmy Material Command), [online] 20 April 2012, http://www.defensemedianetwork.com/stories/ddg-1000s-integrated-power-system-software-hardware-come-together-in-successful-test/

[4] E. Lundquist, “Navy and Industry Pursuing New Power and Propulsion Methods,” (Alion Science Quarterly), 10 June 2009, *wstiac.alionscience.com/pdf/WQV9N1_ART04.pdf*

[5] N. Doerry, “Designing All Electric Ships,” Ninth International Marine Design Conference, Ann Arbor Michigan, 2006

[6] F. Beach, and I. McNab, "Present and Future Naval Applications for Pulsed Power," in *Pulsed Power Conference, 2005 IEEE* , vol., no., pp.1,7, 13-17 June 2005

[7] M. Roa, "ABS Rules for Integrated Power Systems (IPS)," *Electric Ship Technologies Symposium, 2009. ESTS 2009. IEEE* , vol., no., pp.1,17, 20-22 April 2009

[8] Department of Defense Interface Standard Section 300B, *MIL-STD-1399 (NAVY) SECTION 300B,* United States of America, 24 April 2008

[9] Aa. Khaligh, and Z. Li, "Battery, Ultracapacitor, Fuel Cell, and Hybrid Energy Storage Systems for Electric, Hybrid Electric, Fuel Cell, and Plug-In Hybrid Electric Vehicles: State of the Art," *Vehicular Technology, IEEE Transactions on* , vol.59, no.6, pp.2806,2814, July 2010

[10] H. Brandhorst, and Z. Chen, "Achieving a high pulse power system through engineering the battery-capacitor combination," *Applications and Advances, 2001. The Sixteenth Annual Battery Conference on* , vol., no., pp.153,156, 2001

[11] L. Gao, et al. "Active power sharing in hybrid battery/capacitor power sources," *Applied Power Electronics Conference and Exposition, 2003. APEC '03. Eighteenth Annual IEEE* , vol.1, no., pp.497,503 vol.1, 9-13 Feb. 2003

[12] L. Baoquan, et al. "Control method of the transient compensation process of a hybrid energy storage system based on battery and Ultra-capacitor in Micro-grid," *Industrial Electronics (ISIE), 2012 IEEE International Symposium on* , vol., no., pp.1325,1329, 28-31 May 2012

[13] J. McGroarty, et al. "Flywheel energy storage system for electric start and an all-electric ship," *Electric Ship Technologies Symposium, 2005 IEEE* , vol., no., pp.400,406, 25-27 July 2005

[14] M. Mench, *Fuel Cell Engines,* Hoboken, NJ: John Wiley & Sons, 2008

[15] B. Gou, et al. *Fuel Cells Modeling, Control, and Applications*, Boca Raton, FL: CRC Press Taylor & Francis Group, 2010

[16] Sammes, *Fuel Cell Technology reaching towards commercialization.:*Germany: Springer, 2006

[17] K. Duncan, et al. "Dependence of open-circuit potential and power density on electrolyte thickness in solid oxide fuel cells with mixed conducting electrolytes," *Journal of Power Sources*, 2011, vol. 196, issue 5, pp 2445-2451

[18] Curtin, Gangi, *the Business Case for Fuel Cells: Why Top Companies are Purchasing Fuel Cells Today,* Sept. 2010, [Online] Available: http://www.fuelcells.org/wp-content/uploads/2012/02/BusinessCaseforFuelCells.pdf

[19] L. Gao, et al. "An actively controlled fuel cell/battery hybrid to meet pulsed power demands," *Journal of Power Sources,* 2004, no. 130, pp. 202-207 [Online] sciencedirect.com

[20] P. Jones, et al. "A hybrid power source for pulse power applications," *Journal of Power Sources,* 1999, no. 80, pp. 242-247

[21] Lecture 7: Lead-acid batteries, *Power Electronics and Photovoltaic Power Systems Laboratory, University of Colorado,* [online] 2009, http://ecee.colorado.edu/~ecen4517/materials/Battery.pdf

[22] About Li-ion batteries, *Nexeon Co. UK*, [online] http://www.nexeon.co.uk/technology/about-li-ion-batteries/

[23] B. Shrestha, "Cycling Fatigue Induced on Electrochemical Energy Storage Cells as a Result of High C Discharge'" Ph.D. dissertation, Dept. Elect. Eng., Univ. of Texas at Arlington, Arlington, TX, 2013

[24] P. Novak, "High Current Recharge of Electrochemical Cells," Ph.D. dissertation, Dept. Elect. Eng., Univ. of Texas at Arlington, Arlington, TX, 2013

[25] S. Lipka, 'Asymmetric Electrochemical Capacitor Derived from Coal,' http://www.docstoc.com/docs/40855748/Asymmetric-Electrochemical-Capacitor-Derived-from-Coal.

[26] M. Hantel, "Graphite Oxide and Graphene Oxide Based Electrrode Materials for Electrochemical Double Layer Capacitors." Doctor of Sciences, Univ. Technische Universitat Munchen, Germany, 2013

[27] Introducing JM Energy Lithium Ion Capacitor, ULTIMO, http://www.jmenergy.co.jp/en/product.html, Copyright(C) 2009.

[28] JM Energy Lithium Ion Capacitor Presentation, ULTIMO, http://www.jmenergy.co.jp/en/product.html, JM Energy Corporation, Copyright(C), July 2010.

[29] The concept of the Lithium Ion Capacitor, *JSR Micro*, [online] http://www.jsrmicro.be/en/lic_concept

[30] Franklin H. Holcomb, Hybrid-Intelligent POWER “HI-POWER”, 2008 High-Megawatt Power Converter Technology R&D Roadmap Workshop, NIST, Gaithersburg, MD, April 8, 2008.

[31] ‘DS-300W Vertical Axis Wind Turbine,’ http://www.hi-vawt.com.tw/en/ds300w.html, © 2010 Hi-VAWT Technology Corp., April 26, 2012.

[32] ‘SCHOTT PERFORM POLY 235-245 Datasheet,’ http://www.schottsolar.com/us/products/photovoltaics/schott-perform-poly/, ©2012 SCHOTT Solar Inc., April 26, 2012.

[33] ‘FLEXmax 60 Maximum Power Point Tracking Charge Controller Users Manual,’ http://www.outbackpower.com/, 900-0009-01-00 REV A, © 2008 OutBack Power Technologies, Inc.

[34] ‘C40 Xantrex C series - charge controller C40 - 12...48 V DC - load 40A,’ © Schneider Electric, April 26, 2012.

[35] ‘Nexa™ (310-0027) Power Module User’s Manual,’ 5,000,001 Series PBS, © 2003 Ballard Power Systems Inc., Doc. # MAN5100078, Rev. 0E, June 16, 2003.

[36] ‘Zahn Electronics CH100105F-S Buck Converter,’ http://www.zahninc.com/sd15.html, © 2009 by Zahn Electronics, Inc. April 26, 2012.

[37] Diehard Products Marine and RV, http://www.diehard.com/products/marine-and-rv, KCD IP, LLC., April 13, 2012.

[38] ‘Sealed GFX 1424 (60Hz) Low Power Sinewave Inverter,’ © 2008 OutBack Power Technologies, Inc., http://www.outbackpower.com/index.php/outback-products/inverters-chargers/item/sealed-gfx1424?category_id=448

[39] ‘Sealed GTFX2524 (60Hz) Grid Interactive Sinewave Inverter,’ © 2008 OutBack Power Technologies, Inc., [Online] http://www.outbackpower.com/index.php/outback-products/inverters-chargers/item/sealed-gtfx2524?category_id=444

[40] ‘Crydom CSW Panel Mount Series Solid State Relays,’ http://www.crydom.com/en/Products/Catalog/c_s.pdf, ©2012 Crydom Inc., April 26, 2012.

[41] ‘Model 63800 Series Programmable AC&DC Electronic load,’ http://www.chromausa.com/pdf/63800-E.pdf, © 2010 - 2012 Chroma Systems Solutions, Inc., April 26, 2012.

[42] ‘Duro DuroStar DS7200Q 6,000 Watt Diesel Powered Fully Enclosed Portable Generator With Wireless Remote & Electric Start,’ http://www.generatorfactoryoutlet.com/gfo/products/DS7200Q.asp, © 2012 Generator Factory Outlet, April 26,2012.

[43] ‘EU3000is’ *Honda Power Equipment* http://powerequipment.honda.com/generators/models/eu3000is

[44] ‘Crydom CSW Panel Mount Series Solid State Relays,’ http://www.crydom.com/en/Products/Catalog/c_s.pdf, ©2012 Crydom Inc., April 26, 2012.

[45] 'Crydom CSW Panel Mount Series Solid State Relays,'
http://www.crydom.com/en/Products/Catalog/c_s.pdf, ©2012 Crydom Inc., April 26, 2012.

[46] Department of Defense Interface Standard Section 300B, MIL-STD-1399, 1992.

[47] IEEE Recommended Practices and Requirements for Harmonic Control in Electrical Power Systems, IEEE Standard 519, 1992.

[48] IEEE Recommended Practice for Monitoring Electric Power Quality, IEEE Standard 1159, 1992.

Biographical Information

Jay Kelley, born and raised in Grand Prairie, Texas, graduated from Pantego Christian Academy in 2007. Jay chose to attend the University of Texas at Arlington and pursue a degree through the College of Engineering's Electrical Engineering department.

During his undergraduate career, he served as an officer for a variety of student organizations. Among these were the honors societies of Tau Beta Pi, Golden Key, and Eta Kappa Nu. He served for two years as an officer of the electrical engineering professional society student chapter, IEEE, including a term as the chapter president before graduating with a B.S. in Electrical Engineering in 2012.

While still a Junior in the undergraduate curriculum, Jay began working for the newly hired electrical engineering professor, Dr. David Wetz. Work included the construction of the MicroGrid Testbed that would later become part of the foundation for his Master's thesis research, which would conclude in December of 2013.

Jay will receive his Master's in Electrical Engineering from the University of Texas at Arlington in May of 2014. Upon graduation, Jay plans to attend the Cedar Valley Law Enforcement Academy for Texas state law enforcement certification.